Article

Charged jet evolution and the underlying event in proton-antiproton collisions at 1.8 TeV

CDF Collaboration

CLARK, Allan Geoffrey (Collab.), *et al*.

Abstract

The growth and development of “charged particle jets” produced in proton-antiproton collisions at 1.8 TeV are studied over a transverse momentum range from 0.5 GeV/c to 50 GeV/c. A variety of leading (highest transverse momentum) charged jet observables are compared with the QCD Monte Carlo models HERWIG, ISAJET, and PYTHIA. The models describe fairly well the multiplicity distribution of charged particles within the leading charged jet, the size of the leading charged jet, the radial distribution of charged particles and transverse momentum around the leading charged jet direction, and the momentum distribution of charged particles within the leading charged jet. The direction of the leading “charged particle jet” in each event is used to define three regions of η−φ space. The “toward” region contains the leading “charged particle jet,” while the “away” region, on the average, contains the away-side jet. The “transverse” region is perpendicular to the plane of the hard 2-to-2 scattering and is very sensitive to the “underlying event” component of the QCD Monte Carlo models. HERWIG, [...]

Reference

CDF Collaboration, CLARK, Allan Geoffrey (Collab.), *et al*. Charged jet evolution and the underlying event in proton-antiproton collisions at 1.8 TeV. *Physical Review. D*, 2002, vol. 65, no. 09

DOI : 10.1103/PhysRevD.65.092002

Charged jet evolution and the underlying event in proton-antiproton collisions at 1.8 TeV

T. Affolder,[1] H. Akimoto,[2] A. Akopian,[3] M. G. Albrow,[4] P. Amaral,[5] D. Amidei,[6] K. Anikeev,[7] J. Antos,[8] G. Apollinari,[4] T. Arisawa,[2] A. Artikov,[9] T. Asakawa,[10] W. Ashmanskas,[5] F. Azfar,[11] P. Azzi-Bacchetta,[12] N. Bacchetta,[12] H. Bachacou,[1] S. Bailey,[13] P. de Barbaro,[14] A. Barbaro-Galtieri,[1] V. E. Barnes,[15] B. A. Barnett,[16] S. Baroiant,[17] M. Barone,[18] G. Bauer,[7] F. Bedeschi,[19] S. Belforte,[20] W. H. Bell,[21] G. Bellettini,[19] J. Bellinger,[22] D. Benjamin,[23] J. Bensinger,[24] A. Beretvas,[4] J. P. Berge,[4] J. Berryhill,[5] A. Bhatti,[3] M. Binkley,[4] D. Bisello,[12] M. Bishai,[4] R. E. Blair,[25] C. Blocker,[24] K. Bloom,[6] B. Blumenfeld,[16] S. R. Blusk,[14] A. Bocci,[3] A. Bodek,[14] W. Bokhari,[26] G. Bolla,[15] Y. Bonushkin,[27] D. Bortoletto,[15] J. Boudreau,[28] A. Brandl,[29] S. van den Brink,[16] C. Bromberg,[30] M. Brozovic,[23] E. Brubaker,[1] N. Bruner,[29] E. Buckley-Geer,[4] J. Budagov,[9] H. S. Budd,[14] K. Burkett,[13] G. Busetto,[12] A. Byon-Wagner,[4] K. L. Byrum,[25] S. Cabrera,[23] P. Calafiura,[1] M. Campbell,[6] W. Carithers,[1] J. Carlson,[6] D. Carlsmith,[22] W. Caskey,[17] A. Castro,[31] D. Cauz,[20] A. Cerri,[19] A. W. Chan,[8] P. S. Chang,[8] P. T. Chang,[8] J. Chapman,[6] C. Chen,[26] Y. C. Chen,[8] M. -T. Cheng,[8] M. Chertok,[17] G. Chiarelli,[19] I. Chirikov-Zorin,[9] G. Chlachidze,[9] F. Chlebana,[4] L. Christofek,[32] M. L. Chu,[8] Y. S. Chung,[14] C. I. Ciobanu,[33] A. G. Clark,[34] A. Connolly,[1] J. Conway,[35] M. Cordelli,[18] J. Cranshaw,[36] R. Cropp,[37] R. Culbertson,[4] D. Dagenhart,[38] S. D'Auria,[21] F. DeJongh,[4] S. Dell'Agnello,[18] M. Dell'Orso,[19] L. Demortier,[3] M. Deninno,[31] P. F. Derwent,[4] T. Devlin,[35] J. R. Dittmann,[4] A. Dominguez,[1] S. Donati,[19] J. Done,[39] M. D'Onofrio,[19] T. Dorigo,[13] N. Eddy,[32] K. Einsweiler,[1] J. E. Elias,[4] E. Engels Jr.,[28] R. Erbacher,[4] D. Errede,[32] S. Errede,[32] Q. Fan,[14] R. G. Feild,[40] J. P. Fernandez,[4] C. Ferretti,[19] R. D. Field,[41] I. Fiori,[31] B. Flaugher,[4] G. W. Foster,[4] M. Franklin,[13] J. Freeman,[4] J. Friedman,[7] Y. Fukui,[42] I. Furic,[7] S. Galeotti,[19] A. Gallas,[13,*] M. Gallinaro,[3] T. Gao,[26] M. Garcia-Sciveres,[1] A. F. Garfinkel,[15] P. Gatti,[12] C. Gay,[40] D. W. Gerdes,[6] P. Giannetti,[19] V. Glagolev,[9] D. Glenzinski,[4] M. Gold,[29] J. Goldstein,[4] I. Gorelov,[29] A. T. Goshaw,[23] Y. Gotra,[28] K. Goulianos,[3] C. Green,[15] G. Grim,[17] P. Gris,[4] L. Groer,[35] C. Grosso-Pilcher,[5] M. Guenther,[15] G. Guillian,[6] J. Guimaraes da Costa,[13] R. M. Haas,[41] C. Haber,[1] S. R. Hahn,[4] C. Hall,[13] T. Handa,[44] R. Handler,[22] W. Hao,[36] F. Happacher,[18] K. Hara,[10] A. D. Hardman,[15] R. M. Harris,[4] F. Hartmann,[44] K. Hatakeyama,[3] J. Hauser,[27] J. Heinrich,[26] A. Heiss,[44] M. Herndon,[16] C. Hill,[17] K. D. Hoffman,[15] C. Holck,[26] R. Hollebeek,[26] L. Holloway,[32] R. Hughes,[33] J. Huston,[30] J. Huth,[13] H. Ikeda,[10] J. Incandela,[4] G. Introzzi,[19] J. Iwai,[2] Y. Iwata,[43] E. James,[6] M. Jones,[26] U. Joshi,[4] H. Kambara,[34] T. Kamon,[39] T. Kaneko,[10] K. Karr,[38] H. Kasha,[40] Y. Kato,[45] T. A. Keaffaber,[15] K. Kelley,[7] M. Kelly,[6] R. D. Kennedy,[4] R. Kephart,[4] D. Khazins,[23] T. Kikuchi,[10] B. Kilminster,[14] B. J. Kim,[46] D. H. Kim,[46] H. S. Kim,[32] M. J. Kim,[46] S. B. Kim,[46] S. H. Kim,[10] Y. K. Kim,[1] M. Kirby,[23] M. Kirk,[24] L. Kirsch,[24] S. Klimenko,[41] P. Koehn,[33] K. Kondo,[2] J. Konigsberg,[41] A. Korn,[7] A. Korytov,[41] E. Kovacs,[25] J. Kroll,[26] M. Kruse,[23] S. E. Kuhlmann,[25] K. Kurino,[43] T. Kuwabara,[10] A. T. Laasanen,[15] N. Lai,[5] S. Lami,[3] S. Lammel,[4] J. Lancaster,[23] M. Lancaster,[1] R. Lander,[17] A. Lath,[35] G. Latino,[19] T. LeCompte,[25] A. M. Lee IV,[23] K. Lee,[36] S. Leone,[19] J. D. Lewis,[4] M. Lindgren,[27] T. M. Liss,[32] J. B. Liu,[14] Y. C. Liu,[8] D. O. Litvintsev,[4] O. Lobban,[36] N. Lockyer,[26] J. Loken,[11] M. Loreti,[12] D. Lucchesi,[12] P. Lukens,[4] S. Lusin,[22] L. Lyons,[11] J. Lys,[1] R. Madrak,[13] K. Maeshima,[4] P. Maksimovic,[13] L. Malferrari,[31] M. Mangano,[19] M. Mariotti,[12] G. Martignon,[12] A. Martin,[40] J. A. J. Matthews,[29] J. Mayer,[37] P. Mazzanti,[31] K. S. McFarland,[14] P. McIntyre,[39] E. McKigney,[26] M. Menguzzato,[12] A. Menzione,[19] C. Mesropian,[3] A. Meyer,[4] T. Miao,[4] R. Miller,[30] J. S. Miller,[6] H. Minato,[10] S. Miscetti,[18] M. Mishina,[42] G. Mitselmakher,[41] N. Moggi,[31] E. Moore,[29] R. Moore,[6] Y. Morita,[42] T. Moulik,[15] M. Mulhearn,[7] A. Mukherjee,[4] T. Muller,[44] A. Munar,[19] P. Murat,[4] S. Murgia,[30] J. Nachtman,[27] V. Nagaslaev,[36] S. Nahn,[40] H. Nakada,[10] I. Nakano,[43] C. Nelson,[4] T. Nelson,[4] C. Neu,[33] D. Neuberger,[44] C. Newman-Holmes,[4] C.-Y. P. Ngan,[7] H. Niu,[24] L. Nodulman,[25] A. Nomerotski,[41] S. H. Oh,[23] Y. D. Oh,[46] T. Ohmoto,[43] T. Ohsugi,[43] R. Oishi,[10] T. Okusawa,[45] J. Olsen,[22] W. Orejudos,[1] C. Pagliarone,[19] F. Palmonari,[19] R. Paoletti,[19] V. Papadimitriou,[36] D. Partos,[24] J. Patrick,[4] G. Pauletta,[20] M. Paulini,[1,†] C. Paus,[7] D. Pellett,[17] L. Pescara,[12] T. J. Phillips,[23] G. Piacentino,[19] K. T. Pitts,[32] A. Pompos,[15] L. Pondrom,[22] G. Pope,[28] M. Popovic,[37] F. Prokoshin,[9] J. Proudfoot,[25] F. Ptohos,[18] O. Pukhov,[9] G. Punzi,[19] A. Rakitine,[7] F. Ratnikov,[35] D. Reher,[1] A. Reichold,[11] A. Ribon,[12] W. Riegler,[13] F. Rimondi,[31] L. Ristori,[19] M. Riveline,[37] W. J. Robertson,[23] A. Robinson,[37] T. Rodrigo,[47] S. Rolli,[38] L. Rosenson,[7] R. Roser,[4] R. Rossin,[12] C. Rott,[15] A. Roy,[15] A. Ruiz,[47] A. Safonov,[17] R. St. Denis,[21] W. K. Sakumoto,[14] D. Saltzberg,[27] C. Sanchez,[33] A. Sansoni,[18] L. Santi,[20] H. Sato,[10] P. Savard,[37] P. Schlabach,[4] E. E. Schmidt,[4] M. P. Schmidt,[40] M. Schmitt,[13,*] L. Scodellaro,[12] A. Scott,[27] A. Scribano,[19] S. Segler,[4] S. Seidel,[29] Y. Seiya,[10] A. Semenov,[9] F. Semeria,[31] T. Shah,[7] M. D. Shapiro,[1] P. F. Shepard,[28] T. Shibayama,[10] M. Shimojima,[10] M. Shochet,[5] A. Sidoti,[12] J. Siegrist,[1] A. Sill,[36] P. Sinervo,[37] P. Singh,[32] A. J. Slaughter,[40] K. Sliwa,[38] C. Smith,[16] F. D. Snider,[4] A. Solodsky,[3] J. Spalding,[4] T. Speer,[34] P. Sphicas,[7] F. Spinella,[19] M. Spiropulu,[13] L. Spiegel,[4] J. Steele,[22] A. Stefanini,[19] J. Strologas,[32] F. Strumia,[34] D. Stuart,[4] K. Sumorok,[7] T. Suzuki,[10] T. Takano,[45] R. Takashima,[43] K. Takikawa,[10] P. Tamburello,[23] M. Tanaka,[10] B. Tannenbaum,[27] M. Tecchio,[6] R. Tesarek,[4] P. K. Teng,[8] K. Terashi,[3] S. Tether,[7] A. S. Thompson,[21] R. Thurman-Keup,[25] P. Tipton,[14] S. Tkaczyk,[4] D. Toback,[39]K. Tollefson,[14] A. Tollestrup,[4] D. Tonelli,[19] H. Toyoda,[45] W. Trischuk,[37] J. F. de Troconiz,[13] J. Tseng,[7] N. Turini,[19] F. Ukegawa,[10] T. Vaiciulis,[14] J. Valls,[35] S. Vejcik III,[4] G. Velev,[4] G. Veramendi,[1] R. Vidal,[4] I. Vila,[47] R. Vilar,[47] I. Volobouev,[1] M. von der Mey,[27] D. Vucinic,[7] R. G. Wagner,[25] R. L. Wagner,[4] N. B. Wallace,[35] Z. Wan,[35] C. Wang,[23] M. J. Wang,[8] B. Ward,[21] S. Waschke,[21] T. Watanabe,[10] D. Waters,[11] T. Watts,[35] R. Webb,[39] H. Wenzel,[44] W. C. Wester III,[4]

A. B. Wicklund,[25] E. Wicklund,[4] T. Wilkes,[17] H. H. Williams,[26] P. Wilson,[4] B. L. Winer,[33] D. Winn,[6] S. Wolbers,[4] D. Wolinski,[6] J. Wolinski,[30] S. Wolinski,[6] S. Worm,[29] X. Wu,[34] J. Wyss,[19] W. Yao,[1] G. P. Yeh,[4] P. Yeh,[8] J. Yoh,[4] C. Yosef,[30] T. Yoshida,[45] I. Yu,[46] S. Yu,[26] Z. Yu,[40] A. Zanetti,[20] F. Zetti,[1] and S. Zucchelli[31]

(CDF Collaboration)

[1]*Ernest Orlando Lawrence Berkeley National Laboratory, Berkeley, California 94720*
[2]*Waseda University, Tokyo 169, Japan*
[3]*Rockefeller University, New York, New York 10021*
[4]*Fermi National Accelerator Laboratory, Batavia, Illinois 60510*
[5]*Enrico Fermi Institute, University of Chicago, Chicago, Illinois 60637*
[6]*University of Michigan, Ann Arbor, Michigan 48109*
[7]*Massachusetts Institute of Technology, Cambridge, Massachusetts 02139*
[8]*Institute of Physics, Academia Sinica, Taipei, Taiwan 11529, Republic of China*
[9]*Joint Institute for Nuclear Research, RU-141980 Dubna, Russia*
[10]*University of Tsukuba, Tsukuba, Ibaraki 305, Japan*
[11]*University of Oxford, Oxford OX1 3RH, United Kingdom*
[12]*Universita di Padova, Istituto Nazionale di Fisica Nucleare, Sezione di Padova, I-35131 Padova, Italy*
[13]*Harvard University, Cambridge, Massachusetts 02138*
[14]*University of Rochester, Rochester, New York 14627*
[15]*Purdue University, West Lafayette, Indiana 47907*
[16]*The Johns Hopkins University, Baltimore, Maryland 21218*
[17]*University of California at Davis, Davis, California 95616*
[18]*Laboratori Nazionali di Frascati, Istituto Nazionale di Fisica Nucleare, I-00044 Frascati, Italy*
[19]*Istituto Nazionale di Fisica Nucleare, University and Scuola Normale Superiore of Pisa, I-56100 Pisa, Italy*
[20]*Istituto Nazionale di Fisica Nucleare, University of Trieste/Udine, Italy*
[21]*Glasgow University, Glasgow G12 8QQ, United Kingdom*
[22]*University of Wisconsin, Madison, Wisconsin 53706*
[23]*Duke University, Durham, North Carolina 27708*
[24]*Brandeis University, Waltham, Massachusetts 02254*
[25]*Argonne National Laboratory, Argonne, Illinois 60439*
[26]*University of Pennsylvania, Philadelphia, Pennsylvania 19104*
[27]*University of California at Los Angeles, Los Angeles, California 90024*
[28]*University of Pittsburgh, Pittsburgh, Pennsylvania 15260*
[29]*University of New Mexico, Albuquerque, New Mexico 87131*
[30]*Michigan State University, East Lansing, Michigan 48824*
[31]*Istituto Nazionale di Fisica Nucleare, University of Bologna, I-40127 Bologna, Italy*
[32]*University of Illinois, Urbana, Illinois 61801*
[33]*The Ohio State University, Columbus, Ohio 43210*
[34]*University of Geneva, CH-1211 Geneva 4, Switzerland*
[35]*Rutgers University, Piscataway, New Jersey 08855*
[36]*Texas Tech University, Lubbock, Texas 79409*
[37]*Institute of Particle Physics, University of Toronto, Toronto, Canada M5S 1A7*
[38]*Tufts University, Medford, Massachusetts 02155*
[39]*Texas A&M University, College Station, Texas 77843*
[40]*Yale University, New Haven, Connecticut 06520*
[41]*University of Florida, Gainesville, Florida 32611*
[42]*High Energy Accelerator Research Organization (KEK), Tsukuba, Ibaraki 305, Japan*
[43]*Hiroshima University, Higashi-Hiroshima 724, Japan*
[44]*Institut für Experimentelle Kernphysik, Universität Karlsruhe, 76128 Karlsruhe, Germany*
[45]*Osaka City University, Osaka 588, Japan*
[46]*Center for High Energy Physics, Kyungpook National University, Taegu 702-701, Korea, Seoul National University, Seoul 151-742, Korea, and SungKyunKwan University, Suwon 440-746, Korea*
[47]*Instituto de Fisica de Cantabria, CSIC–University of Cantabria, 39005 Santander, Spain*

(Received 6 July 2001; published 22 April 2002)

The growth and development of ''charged particle jets'' produced in proton-antiproton collisions at 1.8 TeV are studied over a transverse momentum range from 0.5 GeV/c to 50 GeV/c. A variety of leading (highest transverse momentum) charged jet observables are compared with the QCD Monte Carlo models HERWIG, ISAJET, and PYTHIA. The models describe fairly well the multiplicity distribution of charged particles within the leading charged jet, the size of the leading charged jet, the radial distribution of charged particles and transverse momentum around the leading charged jet direction, and the momentum distribution of charged particles within the leading charged jet. The direction of the leading ''charged particle jet'' in each event is used to define three regions of η-ϕ space. The ''toward'' region contains the leading ''charged particle jet,'' while the ''away'' region, on the average, contains the away-side jet. The ''transverse'' region is perpendicular to the plane of the hard 2-to-2 scattering and is very sensitive to the ''underlying event'' component of the QCD Monte Carlo models. HERWIG, ISAJET, and PYTHIA with their default parameters do not describe correctly all the properties of the ''transverse'' region.

DOI: 10.1103/PhysRevD.65.092002 PACS number(s): 13.87.Ce, 12.38.Qk, 13.87.Fh

I. INTRODUCTION

In a proton-antiproton collision a large transverse momentum outgoing parton manifests itself as a cluster of particles (both charged and neutral) traveling in roughly the same direction. These clusters are referred to as ''jets.'' In this paper we examine the charged particle component of ''jets.'' Using a simple algorithm, we study clusters of charged particles which we call ''charged particle jets.'' We define the transverse momentum of a ''charged particle jet'' to be the *scalar* sum of the transverse momenta of the charged particles making up the jet. We examine the properties of the leading (highest transverse momentum) ''charged particle jet'' and compare the data with the QCD hard scattering Monte Carlo models HERWIG [1], ISAJET [2], and PYTHIA [3]. Our method of comparing the QCD Monte Carlo models with data is to select a region where the data are very clean so that corrections for experimental effects are small. For this reason, throughout this analysis we consider only charged particles measured by the Collider Detector at Fermilab (CDF) central tracking chamber (CTC) in the region $p_T > 0.5$ GeV/c and $|\eta| < 1$ [4], where the track finding efficiency is high and uniform. In addition to examining the leading ''charged particle jet,'' we study the overall event topology. Figure 1 illustrates the way the QCD Monte Carlo models simulate a proton-antiproton collision in which a hard 2-to-2 parton scattering with transverse momentum, p_T(hard), has occurred. The resulting event contains particles that originate from the two outgoing partons (*plus initial and final-state radiation*) and particles that come from the breakup of the proton and antiproton (i.e., ''beam-beam remnants''). The ''hard scattering'' component consists of the outgoing two ''jets'' plus initial and final-state radiation. The ''underlying event'' is everything except the two outgoing hard scattered ''jets'' and consists of the ''beam-beam remnants'' plus possible contributions from the ''hard scattering'' arising from initial and final-state radiation.

The ''beam-beam remnants'' are what is left over after a parton is knocked out of each of the initial two beam hadrons. It is the reason hadron-hadron collisions are more ''messy'' than electron-positron annihilations and no one really knows how it should be modeled. In the QCD Monte Carlo models the ''beam-beam remnants'' are an important component of the ''underlying event.'' Also, it is possible that multiple parton scattering contributes to the ''underlying event.'' Figure 2 shows the way PYTHIA [3] models the ''underlying event'' in proton-antiproton collision by including multiple parton interactions. In addition to the hard 2-to-2 parton-parton scattering and the ''beam-beam remnants,'' sometimes there is a second ''semi-hard'' 2-to-2 parton-parton scattering that contributes particles to the ''underlying event.''

We use the direction of the leading ''charged particle jet'' in each event to define three regions of η-ϕ space, where η is the pseudorapidity measured along the beam axis and $\Delta\phi$ is the azimuthal angle relative to the leading charged jet [4]. The ''toward'' region contains the leading ''charged particle jet,'' while the ''away'' region, on the average, contains the away-side jet. The ''transverse'' region is perpendicular to the plane of the hard 2-to-2 scattering and is very sensitive to the ''underlying event'' component of the QCD Monte Carlo models. We find that HERWIG, ISAJET, and PYTHIA with their default parameters do not describe correctly all the properties of the ''transverse'' region. For example, none of the models produces the correct p_T dependence of charged particles in the ''transverse'' region.

Of course, from a certain point of view there is no such thing as an ''underlying event'' in a proton-antiproton collision. There is only an ''event'' and one cannot say where a given particle in the event originated. On the other hand, hard scattering collider ''jet'' events have a distinct topology. On the average, the outgoing hadrons ''remember'' the 2-to-2 hard scattering subprocess. An average hard scattering event consists of a collection (or burst) of hadrons traveling roughly in the direction of the initial beam particles and two collections of hadrons (i.e., ''jets'') with large transverse momentum. The two large transverse momentum ''jets'' are roughly back to back in azimuthal angle. Here we use the topological structure of hadron-hadron collisions to study the ''underlying event.'' The ultimate goal is to understand the physics of the ''underlying event,'' but since it is very com-

*Now at Northwestern University, Evanston, Illinois 60208.

†Now at Carnegie Mellon University, Pittsburgh, Pennsylvania 15213.

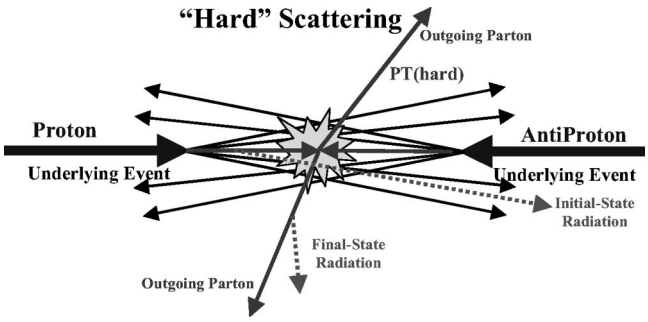

FIG. 1. Illustration of the way the QCD Monte Carlo models simulate a proton-antiproton collision in which a hard 2-to-2 parton scattering with transverse momentum, p_T(hard), has occurred. The resulting event contains particles that originate from the two outgoing partons (*plus initial and final-state radiation*) and particles that come from the breakup of the proton and antiproton (*"beam-beam remnants"*). The ''hard scattering'' component consists of the outgoing two ''jets'' plus initial and final-state radiation. The ''underlying event'' is everything except the two outgoing hard scattered ''jets'' and consists of the ''beam-beam remnants'' plus possible contributions from the ''hard scattering'' arising from initial and final-state radiation.

plicated and involves both non-perturbative as well as perturbative QCD it seems unlikely that this will happen soon. In the mean time, we would like to tune the QCD Monte Carlo models to do a better job fitting the ''underlying event.'' The ''underlying event'' is an unavoidable background to most collider observables and making precise measurements in the collider environment requires accurate modeling of the ''underlying event.''

In Sec. II we discuss the data and the QCD Monte Carlo models used in this analysis and we explain the procedure used to compare the models with the data. In Sec. III, we define ''charged particle jets'' as simple circular regions in η-ϕ space with radius $R=0.7$ and study the growth and development of these jets from $P_T(\text{chgjet1}) \equiv P_{T1}=0.5$ GeV/c to 50 GeV/c. In Sec. IV, we look at the overall event structure by studying correlations in the azimuthal angle $\Delta\phi$ relative to the leading ''charged particle jet.'' In Sec. V we study the behavior of the ''transverse'' region and the ''underlying event.'' We reserve Sec. VI for summary and conclusions.

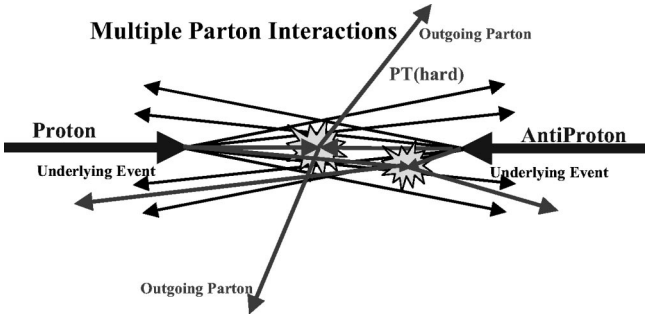

FIG. 2. Illustration of the way PYTHIA models the ''underlying event'' in proton-antiproton collision by including multiple parton interactions. In adddition to the hard 2-to-2 parton-parton scattering with transverse momentum, p_T(hard), there is a second ''semi-hard'' 2-to-2 parton-parton scattering that contributes particles to the ''underlying event.''

II. DATA SELECTION AND MONTE CARLO MODELS

A. Data selection

The CDF detector, described in detail in Ref. [5], measures the trajectories and transverse momenta, p_T, of charged particles contained within the central tracking chamber (CTC), silicon vertex detector (SVX), and vertex time projection chamber (VTX), which are immersed in a 1.4 T solenoidal magnetic field. The energy of neutral particles is measured in the calorimeters, but at the low momenta relevant for this study the efficiency and resolution of the calorimeter is poor.

To remain in a region of high efficiency, this analysis considers only charged particles measured by the CTC with $p_T>0.5$ GeV/c and $|\eta|<1$. In this region the efficiency is high and the momentum resolution is good [$\delta p_T/p_T^2 < 0.002$ (GeV/c)$^{-1}$]. In general, the observed charged particle tracks include some spurious tracks that result from secondary interactions between primary particles, including neutral particles, and the detector material. There are also particles originating from other proton-antiproton collisions in the same bunch crossing. To reduce the contribution from these sources, we do not consider events with two or more identified collision vertices and we consider only tracks which point to the interaction vertex within 2 cm along the beam direction, z. (The beam's luminous region along z has a Gaussian width of 30 cm over which other unidentified collisions could have occurred.) Futhermore, we use only tracks which point within 1 cm transverse to the beam direction, d_0. Detector simulation studies indicate that these cuts are greater than 90% efficient and that the number of remaining spurious tracks is about 3.5%. without the cuts the number of spurious tracks is approximately 9%.

To determine the systematic uncertainty due to remaining spurious tracks, every data point on every plot was determined with three different d_0 cuts: 1 cm, 0.5 cm, and no cut. This widely varies the contribution from spurious tracks. The spread is used as a systematic uncertainty and added in quadrature with the statistical error.

The approach used to compare the Monte Carlo models with data is to select a region where the data are very clean. The track finding efficiency can vary substantially for very low p_T tracks and in dense high p_T jets. To avoid this we considered only the region $p_T>0.5$ GeV/c and $|\eta|<1$ where the track finding efficiency is high (about 92%) and stable, and we consider only charged particle jets with transverse momentum less than 50 GeV/c.

The data are not corrected up for the track finding efficiency. Rather, events generated with the Monte Carlo models are corrected down. For the selected p_T and η region, these corrections are small and essentially independent of p_T and η, which is why the study uses only charged particles in this limited region. This approach is used instead of time consuming full detector simulation because of the large number of Monte Carlo events which must be generated. As a check, full simulation was applied to a subset of the Monte

TABLE I. Data sets and selection criterion for the charged particles used in this analysis.

CDF Data Set	Trigger	Events	Selection
Min-bias	Min-bias trigger	626966	zero or one vertex in $\|z\|<100$ cm $\|z_c-z_v\|<2$ cm, $\|d_0\|<1$ cm $p_T>0.5$ GeV/c, $\|\eta\|<1$
JET20	Calorimeter tower cluster with $E_T>20$ Gev	78682	zero or one vertex in $\|z\|<100$ cm $\|z_c-z_v\|<2$ cm, $\|d_0\|<1$ cm $p_T>0.5$ GeV/c, $\|\eta\|<1$

Carlo models to verify that the resulting change was less than the systematic uncertainty.

The two trigger datasets listed in Table I were used. The minimum bias (min-bias) data were selected by requiring that at least one particle interact with the forward beam-beam counter BBC ($3.4<\eta<5.9$) and at least one particle interact with the backward BBC ($-5.9<\eta<-3.4$). Because the rate for the min-bias trigger is very high (>200 kHz), the accept rate must be limited. That makes it very difficult to know the luminosity normalization for the sample, so cross sections cannot be determined. Instead, we study correlations within the events as a function of the transverse momentum of the leading charged jet, P_{T1}. The JET20 trigger dataset is used to extend the study to higher P_{T1}. The JET20 data were collected by requiring at least 20 GeV of energy (*charged plus neutral*) in a cluster of calorimeter cells. However, we do not use the calorimeter information. Instead we look only at the charged particles measured in the CTC in the exactly the same way we do for the min-bias data. The JET20 data is, of course, biased for low p_T jets and we do not show the JET20 data below P_{T1} around 20 GeV/c. At large P_{T1} values the JET20 data becomes unbiased and, in fact, we know this occurs at around 20 GeV/c because it is here that it agrees with the (*unbiased*) min-bias data (for example, see Fig. 4).

B. The QCD hard scattering Monte Carlo models

In this analysis, the data are compared with the QCD hard scattering Monte Carlo models HERWIG 5.9, ISAJET 7.32, PYTHIA 6.115, and PYTHIA 6.125. The QCD perturbative 2-to-2 parton-parton differential cross section diverges as the transverse momentum of the scattering, p_T(hard), goes to zero. One must set a minimum p_T(hard)large enough that the resulting cross section is not larger that the total inelastic cross section, and also large enough to ensure that QCD perturbation theory is applicable. In this analysis use the default parameters of the QCD Monte Carlo models and take $p_T(\text{hard})>3$ GeV/c.

Each of the QCD Monte Carlo approaches models the ''beam-beam remnants'' in slightly different ways. However, all the models assume that a hard scattering event is basically the superposition of a hard parton-parton interaction on top of a ''soft'' collision. HERWIG assumes that the ''beam-beam remnants'' are a ''soft'' collision between the two beam ''clusters.'' ISAJET uses a model similar to the one it uses for ''soft'' min-bias events (i.e., ''cut Pomeron''), but with different parameters, to describe the ''beam-beam remnants.'' PYTHIA assumes that each incoming beam hadron leaves behind ''beam remnants,'' which do not radiate initial state radiation, and simply pass through unaffected by the hard process. However, unlike HERWIG and ISAJET, PYTHIA also uses multiple parton interactions to enhance the activity of the ''underlying event'' as illustrated in Fig. 2.

CDF data [6] show evidence for multiple parton collisions in which both interactions are hard. However, in PYTHIA multiple parton collisions contribute to the ''underlying event'' when one scattering is hard (i.e., the outgoing jets) and one scattering is ''soft'' or ''semi-hard.'' This second ''semi-hard'' collision cannot be computed reliably by perturbation theory and must be modeled. The amount of ''soft'' or ''semi-hard'' multiple parton scattering is essentially arbitrary. In this analysis we examine two versions of PYTHIA, PYTHIA 6.115 and PYTHIA 6.125 both with the default values for all the parameters. The default values of the parameters are different in version 6.115 and 6.125. In particular, the effective minimum transverse momentum for multiple parton interactions, PARP(81), changed from 1.4 GeV/c in version 6.115 to 1.9 GeV/c in version 6.125. Increasing this cutoff decreases the multiple parton interaction cross section which reduces the amount of multiple parton scattering. For completeness, we also consider PYTHIA with no multiple parton scattering [MSTP(81)=0].

Since ISAJET employs independent fragmentation within the leading log framework, it is possible to trace particles back to their origin. Within ISAJET particles can be divided into three categories: particles that arise from the breakup of the beam particles (''beam-beam remnants''), particles that arise from initial-state radiation, and particles that result from the outgoing hard scattering jets plus final-state radiation. The ''hard scattering'' component consists of the particles that arise from the outgoing hard scattering jets plus initial and final-state radiation (the sum of the last two categories). Particles from the first two categories (''beam-beam remnants'' plus initial-state radiation) contribute to the ''underlying event.'' Of course, these categories are not directly distinguishable experimentally. Experimentally one cannot say where a given particle originated. Nevertheless, it is instructive to examine how particles from various origins within ISAJET affect the experimental observables.

Since PYTHIA does not use independent fragmentation, it is not possible to distinguish particles that arise from initial-state radiation from those that arise from final-state radiation

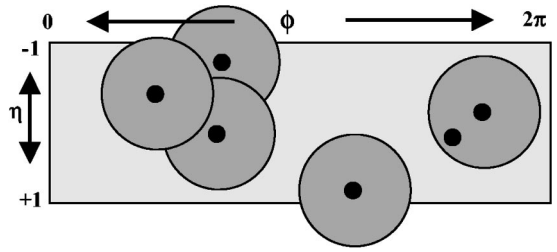

FIG. 3. Illustration of an event with six charged particles ($p_T > 0.5$ GeV/c and $|\eta| < 1$) and five charged jets (circular regions in η-ϕ space with $R = 0.7$).

(*as is true in nature*), but we can identify the ''beam-beam remnants.'' When, for example, a color string within PYTHIA breaks into hadrons it is not possible to say which of the two partons producing the string was the parent. For HERWIG and PYTHIA we divide particles into two categories: particles that arise from the breakup of the beam particles (''beam-beam remnants''), and particles that result from the outgoing hard scattering jets plus initial and final-state radiation (''hard scattering component''). For PYTHIA we include particles that arise from the ''soft'' or ''semi-hard'' scattering in multiple parton interactions in the ''beam-beam remnant'' component.

In comparing the QCD Monte Carlo models with the data, we require that the Monte Carlo events satisfy the CDF min-bias trigger and we apply a 92% correction for the CTC track finding efficiency (i.e., 8% of the charged tracks are, on the average, removed). The Monte Carlo model predictions have an uncertainty (statistical plus systematic) of about 5%.

Requiring the Monte Carlo events to satisfy the min-bias trigger is important when comparing with the min-bias data, but does not matter when comparing with the JET20 data since essentially all high p_T jet events satisfy the min-bias trigger. However, restricting ourselves to the ''clean'' region $p_T > 0.5$ GeV/c and $|\eta| < 1$ means, of course, that we see, on the average, only a small fraction of the total number of charged particles that are produced in the event. For example, of the 74 charged particles produced, on the average, by ISAJET [with $p_T(\text{hard}) > 3$ GeV/c] at 1.8 TeV in proton-antiproton collisions about 25 have $p_T > 0.5$ GeV/c; about 14 have $|\eta| < 1$; and only about 5 charged particles are, on the average, in the region $p_T > 0.5$ GeV/c and $|\eta| < 1$. However, at large values of P_{T1} we are selecting events with many charged particles in the region $p_T > 0.5$ GeV/c and $|\eta| < 1$ allowing us to study the topology of the event in detail.

III. THE EVOLUTION OF ''CHARGED PARTICLE JETS''

In this section, we define ''charged particle jets'' and examine the evolution of these jets from $P_T(\text{chgjet1}) \equiv P_{T1} = 0.5$ GeV/c to 50 GeV/c. As illustrated in Fig. 3, we define ''jets'' as clusters of charged particles in circular regions ($R = 0.7$) of η-ϕ space. No attempt is made to correct the ''jets'' for contributions from the ''underlying event.'' Also every charged particle in the event is assigned to a jet, with the possibility that some jets might consist of just one charged particle. We use this simple, but non-standard jet definition since we will be dealing with jets that consist of only a few low p_T charged particles or even a single low p_T particle. The standard CDF jet algorithm based on calorimeter energy clustering is not directly applicable to charged particles. Furthermore, we need an algorithm that can be applied at low transverse momentum.

A. Charged particle jet definition

We define ''jets'' as circular regions in η-ϕ space with radius defined by $R = \sqrt{(\Delta\eta)^2 + (\Delta\phi)^2}$. Our jet algorithm is as follows:

Order all charged particles according to their p_T.

Start with the highest p_T particle and include in the jet all particles within the radius $R = 0.7$ (considering each particle in the order of decreasing p_T and recalculating the centroid of the jet after each new particle is added to the jet).

Go to the next highest p_T particle (not already included in a jet) and add to the jet all particles (not already included in a jet) within $R = 0.7$.

Continue until all particles are in a jet.

We consider all charged particles ($p_T > 0.5$ GeV/c and $|\eta| < 1$) and allow the jet radius to extend outside $|\eta| < 1$. Figure 3 illustrates an event with six charged particles and five jets. We define the transverse momentum of the jet to be the *scalar* p_T sum of all the particles within the jet, where p_T is measured with respect to the beam axis [4]. The charged particle jets are ordered according to their transverse momentum with P_{T1} being the jet with the largest transverse momentum. The maximum possible number of jets is related to the geometrical size of jets compared to the size of the region considered and is given approximately by

$$N_{jet}(\max) \approx 2\frac{(2)(2\pi)}{\pi(0.7)^2} \approx 16. \tag{1}$$

The additional factor of two is to allow for the possible overlap of jet radii as illustrated in Fig. 3.

We realize that the simple charged particle jet definition used here is not theoretically favored since if applied at the parton level it is not infrared safe. Of course, all jet definitions (and in fact all observables) are infrared safe at the hadron level. Some of the observables presented here do, of course, depend on the definition of a jet and it is important to apply the same definition to both the QCD Monte Carlo models and the data.

B. Leading charged jet multiplicity

Figure 4 shows the average number of charged particles ($p_T > 0.5$ GeV/c and $|\eta| < 1$) within chgjet1 (leading charged jet) as a function of of its transverse momentum, P_{T1}. The solid points are min-bias data and the open points are the JET20 data. The JET20 data connect smoothly to the min-bias data and this allows us to study observables over the range 0.5 GeV/c $< P_{T1} <$ 50 GeV/c. The errors on the data include both statistical and correlated systematic uncertainties, however the data have not been corrected for efficiency. Figure 4 shows a sharp rise in the leading charged jet multiplicity at low P_{T1} and then a more gradual rise at high P_{T1}. The data are compared with the QCD Monte Carlo

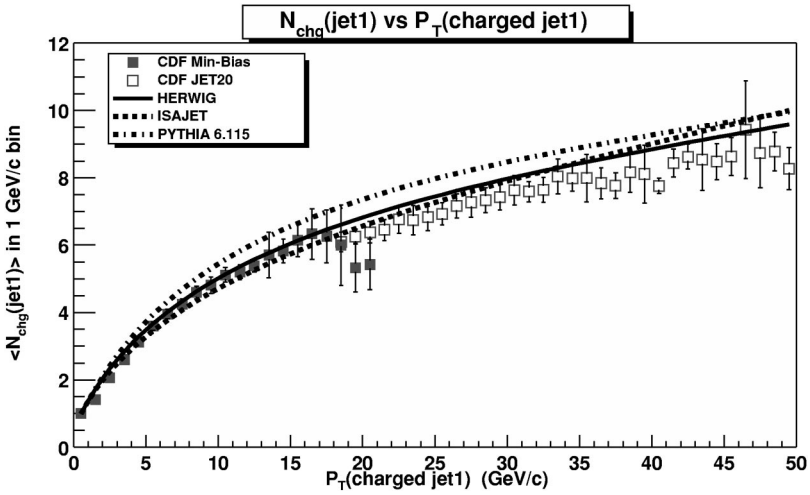

FIG. 4. The average number of charged particles ($p_T>0.5$ GeV/c, $|\eta|<1$) within the leading charged jet ($R=0.7$) as a function of the transverse momentum of the leading charged jet compared with the QCD Monte Carlo models predictions of HERWIG, ISAJET, and PYTHIA 6.115. The solid (open) points are min-bias (JET20) data.

model predictions of HERWIG, ISAJET, and PYTHIA. The theory curves are corrected for the track finding efficiency and have an uncertainty (statistical plus systematic) of around 5%.

Figure 5 shows the multiplicity distribution of the charged particles within chgjet1 (leading charged jet) for $P_{T1}>5$ GeV/c, and 30 GeV/c compared with the QCD Monte Carlo model predictions. Below 5 GeV/c the probability that the leading charged jet consists of just one particle becomes large. The Monte Carlo models agree fairly well with the data at both 5 GeV/c and 30 GeV/c.

C. Leading charged jet "size"

Although we defined jets as circular regions in η-ϕ space with $R=0.7$, this is not necessarily the "size" of the jet. The size of a jet can be defined in many ways. Here we define the size of a jet in two ways, according to particle number or according to transverse momentum. The first corresponds to the radius in η-ϕ space that contains 80% of the charged particles in the jet and the second corresponds to the radius in η-ϕ space that contains 80% of the jet transverse momentum. The data on the average jet size of the leading charged particle jet are compared with the QCD Monte Carlo model predictions of HERWIG, ISAJET, and PYTHIA in Fig. 6. A leading 20 GeV/c charged jet has 80% of its charged particles contained, on the average, within a radius in η-ϕ space of about 0.33, and 80% of its transverse momentum contained, on the average, within a radius of about 0.20. Figure 6 clearly shows the "hot core" of charged jets. The radius containing 80% of the transverse momentum is smaller than the radius that contains 80% of the particles. Furthermore, the radius containing 80% of the transverse momentum decreases as the overall transverse momentum of the jet increases due to limited momentum perpendicular to the jet direction.

We can study the radial distribution of charged particles and transverse momentum within the leading jet by examining the distribution of $\langle N_{\rm chg}\rangle$ and $\langle P_T \text{ sum}\rangle$ as a function of the distance in η-ϕ space from the leading jet direction as illustrated in Fig. 7. Figure 8 and Fig. 9 compare data on the radial multiplicity distribution and the radial transverse momentum distribution, for $P_{T1}>5$ GeV/c and 30 GeV/c compared with the QCD Monte Carlo model predictions. For an average charged jet with $P_{T1}>5$ GeV/c (>30 GeV/c), 80% of the jet p_T lies within $R=0.36$ (0.18). Note that because of QCD fluctuations the average jet size shown in Fig. 6 is not exactly the same as the size of an average jet shown in Figs. 8 and 9.

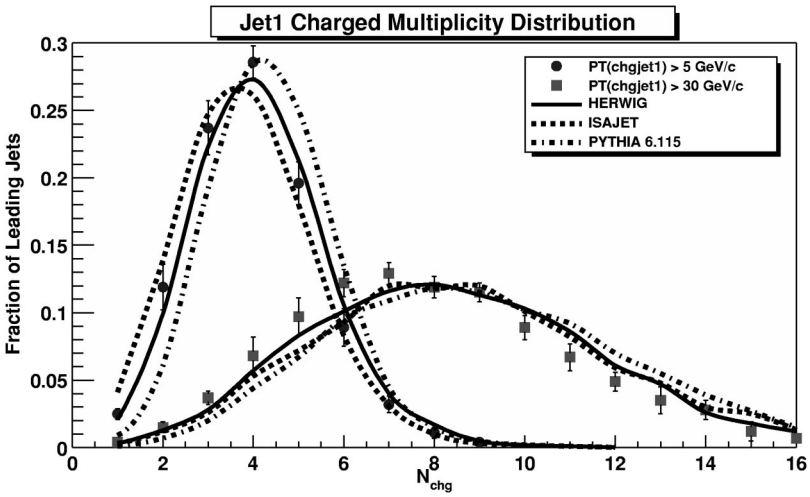

FIG. 5. Multiplicity distribution of charged particles ($p_T>0.5$ GeV/c, $|\eta|<1$) within chgjet1 (leading charged jet) for $P_{T1}>5$ and 30 GeV/c compared with the QCD Monte Carlo model predictions of HERWIG, ISAJET, and PYTHIA 6.115. This plot shows the percentage of events in which the leading charged jet ($R=0.7$) contains $N_{\rm chg}$ charged particles. The $P_{T1}>5$ GeV/c points are min-bias data and the $P_{T1}>30$ GeV/c points are JET20 data.

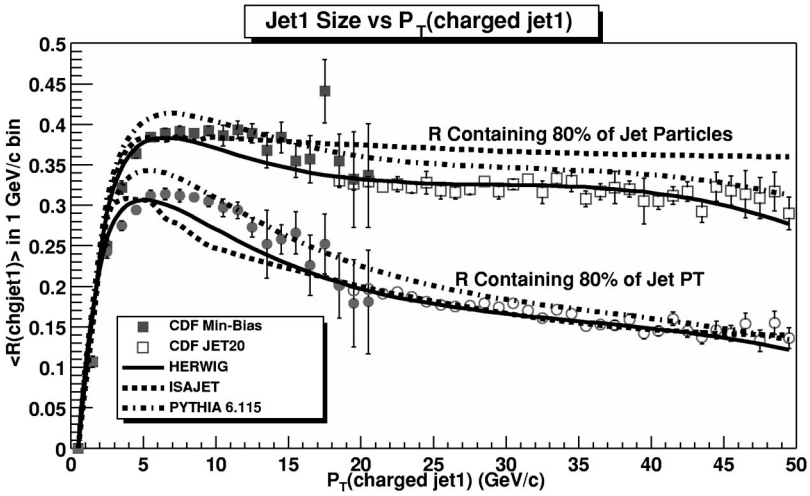

FIG. 6. The average radius in η-ϕ space containing 80% of the charged particles (and 80% of the charged *scalar* p_T sum) as a function of the transverse momentum of the leading charged jet compared with the QCD Monte Carlo model predictions of HERWIG, ISAJET, and PYTHIA 6.115. The solid (open) points are min-bias (JET20) data.

D. Momentum distribution of charged particles within charged jet 1

We define a charged jet fragmentation function, $F(z)$, which describes the momentum distribution of charged particles within the leading charged particle jet. The function $F(z)$ is the number of charged particles between z and $z+dz$ (i.e., the charged particle number density), where $z=p/P(\text{chgjet1})$ is the fraction of the overall charged particle momentum of the jet carried by the charged particle with momentum p. The integral of $F(z)$ over z is the average multiplicity of charged particles within the jet. We refer to this as a fragmentation function, however it is not a true fragmentation function since we are dealing only with charged particle jets.

Figure 10 shows the data on $F(z)$ for $P_{T1}>2$ GeV/c, 5 GeV/c, and 30 GeV/c. The data roughly scale for $P_{T1}>5$ GeV/c and $z>0.1$, with the growth in multiplicity coming from the soft particles (i.e., low z region). This is exactly the behavior expected from a fragmentation function [7]. Figure 11 and Fig. 12 compare data on the $F(z)$ for $P_{T1}>5$ and 30 GeV/c, respectively, with the QCD Monte Carlo model predictions of HERWIG, ISAJET, and PYTHIA.

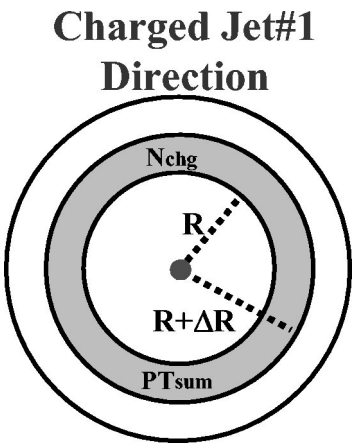

FIG. 7. Illustration of correlations in the radial distance R in η-ϕ space from the direction of the leading charged jet in the event, chgjet1. The average number of charged particles and the average *scalar* p_T sum of charged particles is plotted versus R, where R is the distance in η-ϕ space between the leading charged jet and a charged particle, $R^2=(\Delta\eta)^2+(\Delta\phi)^2$.

The QCD Monte Carlo models describe quite well the multiplicity distribution of charged particles within the leading jet (Fig. 5), the size of the leading jet (Fig. 6), the radial distribution of charged particles and transverse momentum around the leading jet direction (Fig. 8, Fig. 9), and the momentum distribution of charged particles within the leading jet (Fig. 11, Fig. 12). We now proceed to study the overall event structure as a function of transverse momentum of the leading charged jet.

IV. THE OVERALL EVENT STRUCTURE

In the previous section we studied leading charged jet observables. The QCD Monte Carlo models did not have to describe correctly the overall event in order to fit the observable. They only had to describe correctly the properties of the leading charged particle jet, and all the models fit the data fairly well (*although not perfectly*). Now we study observables which test the capacity of the models to describe correctly the overall event structure.

A. Overall charged multiplicity

Figure 13 shows the average number of charged particles in the event with $p_T>0.5$ GeV/c and $|\eta|<1$ (including chgjet1) as a function of P_{T1} (leading charged jet) for the min-bias and JET20 data. Again the JET20 data connect smoothly to the min-bias data and there is a small overlap region where the min-bias and JET20 data agree. Figure 13 shows a sharp rise in the overall charged multiplicity at low P_{T1} and then a more gradual rise at high P_{T1} similar to Fig. 4. We now investigate where these charged particles are located relative to the direction of the leading charged particle jet.

B. Correlations in $\Delta\phi$ relative to charged jet1

As illustrated in Fig. 14, the angle $\Delta\phi=\phi-\phi_{\text{chgjet1}}$ is defined to be the relative azimuthal angle between a charged

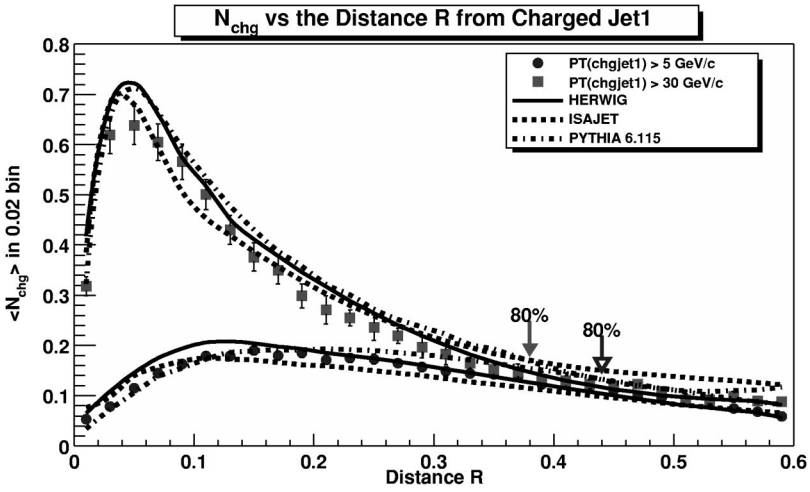

FIG. 8. Charged multiplicity distribution in the radial distance R in η-ϕ space from chgjet1 (leading charged jet) for charged particles with $p_T>0.5$ GeV/c and $|\eta|<1$ when $P_{T1}>5$ and 30 GeV/c. The points are $\langle N_{\rm chg}\rangle$ in a $\Delta R=0.02$ bin (see Fig. 7). The $P_{T1}>5$ GeV/c points are min-bias data and the $P_{T1}>30$ GeV/c points are JET20 data. The data are compared with the QCD Monte Carlo model predictions of HERWIG, ISAJET, and PYTHIA 6.115. For an average charged jet with $P_{T1}>5$ GeV/c (>30 GeV/c), 80% of the charged particles lie within $R=0.44$ (0.38) as marked by the arrows.

particle and the direction of the leading charged particle jet. When we plot $\langle N_{\rm chg}\rangle$ and $\langle P_T$ sum$\rangle$ as a function of $\Delta\phi$, we include all charged particles with $p_T>0.5$ GeV/c and $|\eta|<1$ (including those in chgjet1), where p_T is measured with respect to the beam axis. Figure 15 and Fig. 16 shows the data on the charged multiplicity distribution and transverse momentum distribution, respectively, in the azimuthal angle $\Delta\phi$ relative to the leading charged particle jet for $P_{T1}>2$ GeV/c, 5 GeV/c, and 30 GeV/c.

Figure 17 and Fig. 18 compare the data on the azimuthal distribution of charged multiplicity and transverse momentum relative to the leading charged particle jet with the QCD Monte Carlo model predictions of HERWIG, ISAJET, and PYTHIA for $P_{T1}>5$ GeV/c and Fig. 19 and Fig. 20 for $P_{T1}>30$ GeV/c. Here one sees differences between the three QCD Monte Carlo models and they do not agree as well with these observables as they did with the leading jet observables. The kink in data and the Monte Carlo model predictions around $\Delta\phi=40°$ arises from the cone size choice of $R=0.7$ which we used in defining the charged particle jets.

In Fig. 15 and Fig. 16 we have labeled the region $|\Delta\phi|<60°$ ($|\eta|<1$) as ''toward'' and the region $|\Delta\phi|>120°$ ($|\eta|<1$) as ''away.'' The ''transverse'' region is defined by $60°<|\Delta\phi|<120°$ ($|\eta|<1$). Figure 15 and Fig. 16 show a rapid growth in the ''toward'' and ''away'' region as P_{T1} increases since the ''toward'' region contains the leading charged particle jet, while the ''away'' region, on the average, contains the away-side jet. The ''transverse'' region is perpendicular to the plane of the hard 2-to-2 scattering and, as we will see in Sec. V, is very sensitive to the ''underlying event'' component of the QCD Monte Carlo models.

Figure 21 shows the data on the average number of charged particles ($p_T>0.5$ GeV/c and $|\eta|<1$) as a function of P_{T1} for the three regions. Each point corresponds to the ''toward,'' ''transverse,'' or ''away'' $\langle N_{\rm chg}\rangle$ in a 1 GeV/c bin. The solid points are min-bias data and the open points are JET20 data. The data in Fig. 21 define the average event shape. For example, for a proton-antiproton collider event at 1.8 TeV with $P_{T1}=20$ GeV/c there are, on the average, 8.7 charged particles ''toward'' chgjet1 (including the particles in chgjet1), 2.5 ''transverse'' to chgjet1, and 4.9 ''away'' from chgjet1. Of course, $\langle N_{\rm chg}\rangle$ in all three regions is forced to go to zero as P_{T1} goes to zero. If the leading charged particle jet has no particles then there are no charged particles anywhere.

Figure 22 shows the data on the average *scalar* p_T sum of charged particles ($p_T>0.5$ GeV/c and $|\eta|<1$) as a function of P_{T1} for the three regions. Each point corresponds to the ''toward,'' ''transverse,'' or ''away'' $\langle P_T$ sum$\rangle$ in a 1 GeV/c bin. We will now examine more closely these three regions.

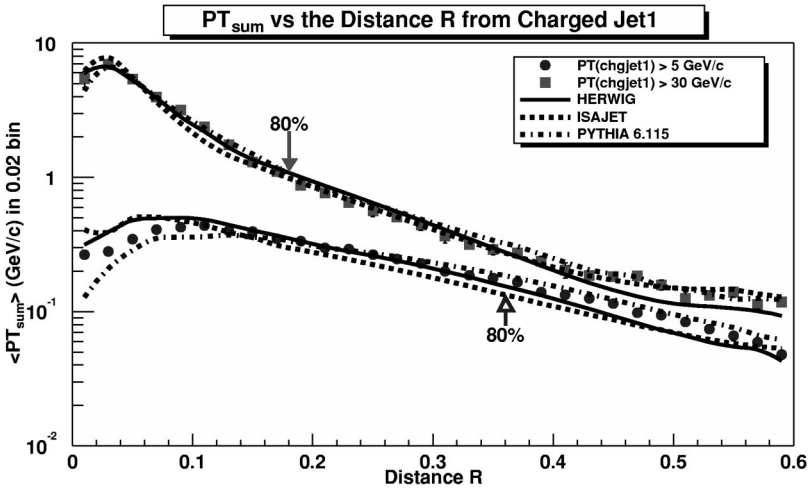

FIG. 9. Charged *scalar* p_T sum distribution in the radial distance R in η-ϕ space from chgjet1 (leading charged jet) for charged particles with $p_T>0.5$ GeV/c and $|\eta|<1$ when $P_{T1}>5$ GeV/c and 30 GeV/c. The points are $\langle P_T$ sum$\rangle$ in a $\Delta R=0.02$ bin (see Fig. 7). The $P_{T1}>5$ GeV/c points are min-bias data and the $P_{T1}>30$ GeV/c points are JET20 data. The data are compared with the QCD hard scattering Monte Carlo model predictions of HERWIG, ISAJET, and PYTHIA 6.115. For an average charged jet with $P_{T1}>5$ GeV/c (>30 GeV/c), 80% of the jet p_T lies within $R=0.36$ (0.18) as marked by the arrows.

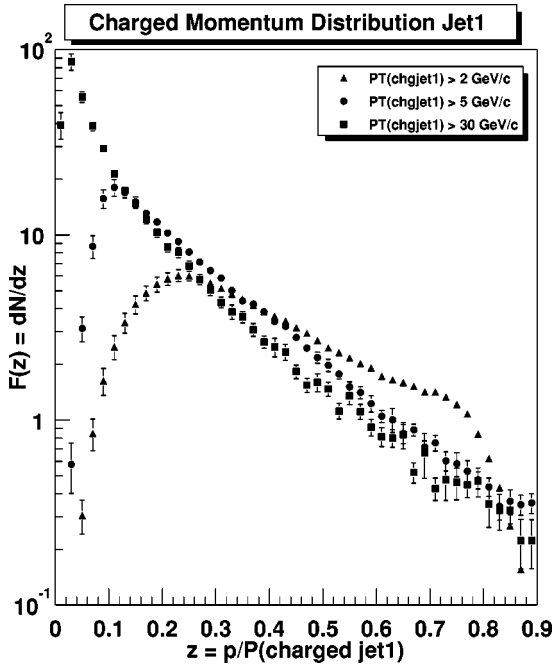

FIG. 10. Momentum distribution of charged particles ($p_T > 0.5$ GeV/c, $|\eta|<1$) within chgjet1 (leading charged jet). The points are the charged number density, $F(z)=dN_{\rm chg}/dz$, where $z = p/P$(chgjet1) is the ratio of the charged particle momentum to the charged momentum of chgjet1. The integral of $F(z)$ is the average number of particles within chgjet1 (see Fig. 5). The $P_{T1} > 2$ GeV/c and 5 GeV/c points are min-bias data and the $P_{T1} > 30$ GeV/c points are JET20 data.

C. The "toward" and "away" regions

Figure 23 shows the data from Fig. 21 on the average number of "toward" region charged particles compared with the QCD Monte Carlo model predictions of HERWIG, ISAJET, and PYTHIA. This plot is very similar to the average number of charged particles within the leading jet shown in Fig. 4. At $P_{T1}=20$ GeV/c the "toward" region contains, on the average, about 8.7 charged particles with about 6.9 of these charged particles belonging to chgjet1. We expect the "toward" region to be dominated by the leading charged particle jet. This is clearly the case for ISAJET as can be seen in Fig. 24 where the predictions of ISAJET for the "toward" region are divided into three categories: charged particles that arise from the breakup of the beam particles ("beam-beam remnants"), charged particles that arise from initial-state radiation, and charged particles that result from the outgoing jets plus final-state radiation. For P_{T1} values below 5 GeV/c the "toward" region charged multiplicity arises mostly from the "beam-beam remnants," but as P_{T1} increases the contribution from the outgoing jets plus final state-radiation quickly begins to dominate. The bump in the "beam-beam remnant" contribution at low P_{T1} is caused by leading jets composed almost entirely from the remnants. Of course, the origin of an outgoing particle ("beam-beam remnant" or "initial-state radiation") is not an experimental observable. Experimentally one cannot say where a given particle comes from. However, we do know the origins of particles generated by the QCD Monte Carlo models and Fig. 23 shows the composition of the "toward" region as modeled by ISAJET.

Figure 25 shows the data from Fig. 21 on the average number of "away" region charged particles compared with the QCD Monte Carlo model predictions of HERWIG, ISAJET, and PYTHIA. In Fig. 26 the data from Fig. 22 on the average *scalar* p_T sum in the "away" region is compared to the QCD Monte Carlo model predictions. The "away" region should be a mixture of the "underlying event" and the away-side outgoing hard scattering jet. This can be seen in Fig. 27 where the predictions of ISAJET for the "away" region are divided into three categories: "beam-beam remnants," initial-state radiation, and outgoing jets plus final-state radiation. For ISAJET the "underlying event" plays a more important role in the "away" region than in the "toward" region since the away-side outgoing hard scattering jet is sometimes outside the region $|\eta|<1$. For the "toward" region ISAJET predicts that the contribution from the outgoing jets plus final state-radiation dominates for P_{T1} values above about 5 GeV/c, whereas for the "away" region this does not occur until around 20 GeV/c.

Both the "toward" and "away" regions are described moderately well by the QCD Monte Carlo models. In the models, these regions are dominated by the outgoing hard scattering jets and as we saw in Sec. III the Monte Carlo models describe the leading outgoing jets fairly accurately. We will now study the "transverse" region, which for the QCD Monte Carlo models is dominated by the "underlying event."

V. THE "TRANSVERSE" REGION AND THE "UNDERLYING EVENT"

The "transverse" region in Fig. 14 is roughly normal to the plane of the 2-to-2 hard scattering and as can be seen in Fig. 21 contains, on the average, considerably fewer charged particles than the "toward" and "away" region. However, there is a lot more activity in the "transverse" region than one might naively expect. If we suppose that the "transverse" multiplicity is uniform in azimuthal angle ϕ and pseudorapidity η, the observed 2.3 charged particles at $P_{T1}=20$ GeV/c translates into 3.8 charged particles per unit pseudorapidity with $p_T>0.5$ GeV/c (multiply by 3 to get 360°, divide by 2 for the two units of η covered in this analysis, multiply by 1.09 to correct for the track finding efficiency). We know that if we include all $p_T>50$ MeV/c that there are, on the average, about four charged particles per unit rapidity in a "soft" proton-antiproton collision at 1.8 TeV [8]. The data in Fig. 21 imply that in the "underlying event" of a hard scattering there are, on the average, about 3.8 charged particles per unit rapidity with $p_T>0.5$ GeV/c. Extrapolating to low p_T assuming the form e^{-2p_T} (which roughly fits the data in Fig. 37) implies that there are roughly 10 charged particles per unit pseudorapidity with $p_T>0$ in the "underlying event" (factor of e). Since we examine only those charged particles with $p_T>0.5$ GeV/c, we cannot accurately extrapolate to low p_T, however, it is clear that the "underlying event" in a hard scattering process has a charged particle density that is at least a factor of two larger

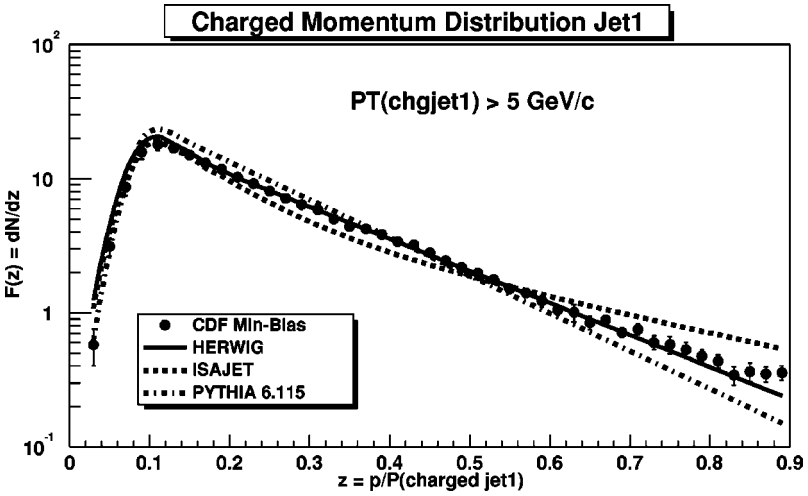

FIG. 11. Data from Fig. 10 on the momentum distribution of charged particles ($p_T > 0.5$ GeV/c, $|\eta| < 1$) within chgjet1 (leading charged jet) for $P_{T1} > 5$ GeV/c compared with the QCD Monte Carlo model predictions of HERWIG, ISAJET, and PYTHIA 6.115.

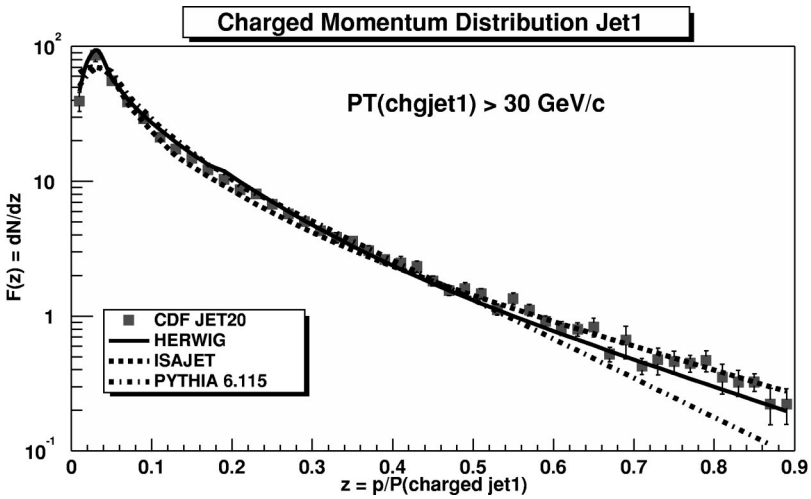

FIG. 12. Data from Fig. 10 on the momentum distribution of charged particles ($p_T > 0.5$ GeV/c, $|\eta| < 1$) within chgjet1 (leading charged jet) for $P_{T1} > 30$ GeV/c compared with the QCD hard scattering Monte Carlo model predictions of HERWIG, ISAJET, and PYTHIA 6.115.

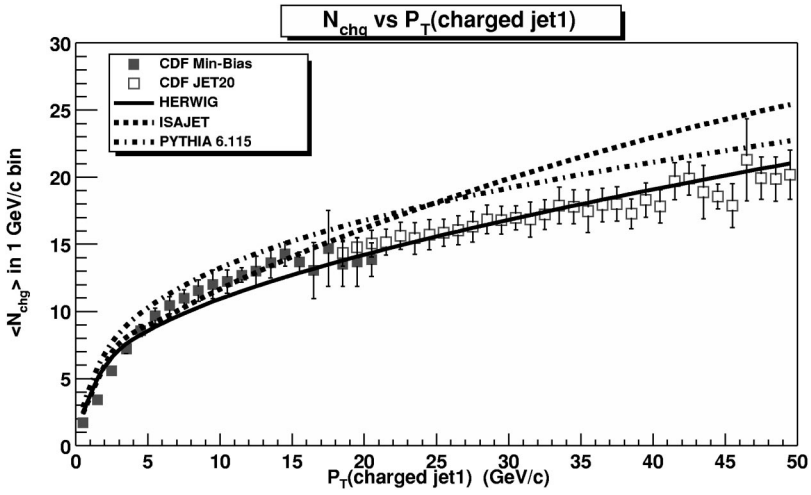

FIG. 13. The average number charged particles in the event ($p_T > 0.5$ GeV/c, $|\eta| < 1$, including chgjet1) as a function of the transverse momentum of the leading charged jet. The solid (open) points are the min-bias (JET20) data. The data are compared with the QCD Monte Carlo model predictions of HERWIG, ISAJET, and PYTHIA 6.115.

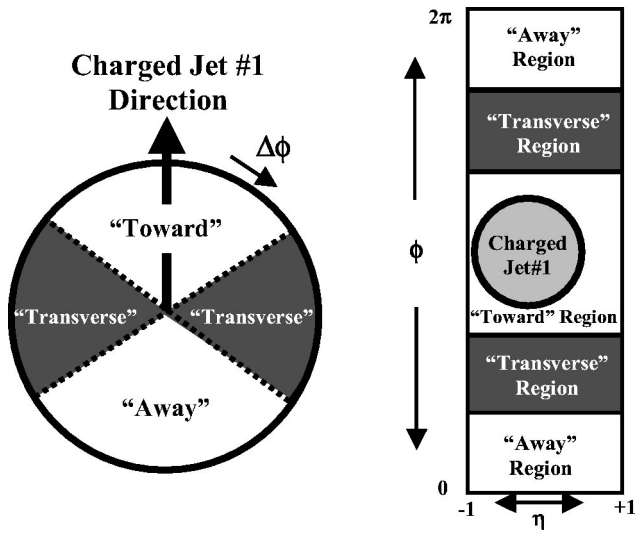

FIG. 14. Illustration of correlations in azimuthal angle $\Delta\phi$ relative to the direction of the leading charged jet in the event, chgjet1. The angle $\Delta\phi=\phi-\phi_{\mathrm{chgjet1}}$ is the relative azimuthal angle between charged particles and the direction of chgjet1. The''toward'' region is defined by $|\Delta\phi|<60°$ and $|\eta|<1$ (includes particles in chgjet1), while the ''away'' region is $|\Delta\phi|>120°$ and $|\eta|<1$. The ''transverse'' region is defined by $60°<|\Delta\phi|<120°$ and $|\eta|<1$. Each region has an area in η-ϕ space of $4\pi/3$. The average number of charged particles, $\langle N_{\mathrm{chg}}\rangle$, and the average *scalar* p_T sum of charged particles, $\langle P_T \text{ sum}\rangle$, in each region are plotted versus the transverse momentum of the leading charged jet.

than the four charged particles per unit rapidity seen in ''soft'' proton-antiproton collisions at this energy. Figure 21 shows that the average number of charged particles in the ''transverse'' region doubles in going from $P_{T1}=1.5$ GeV/c to 2.5 GeV/c and then forms an approximately constant plateau for $P_{T1}>5$ GeV/c.

A. "Transverse" N_{chg} and P_T sum

Figure 28 and Fig. 29 compare the ''transverse'' $\langle N_{\mathrm{chg}}\rangle$ and the ''transverse'' $\langle P_T \text{ sum}\rangle$, respectively, with the QCD Monte Carlo model predictions of HERWIG, ISAJET, and PYTHIA. Figure 30 and Fig. 31 compare the ''transverse'' $\langle N_{\mathrm{chg}}\rangle$ and the ''transverse'' $\langle P_T \text{ sum}\rangle$, respectively, with three versions of PYTHIA (6.115, 6.125, and no multiple scattering). PYTHIA with no multiple parton scattering does not have enough activity in the ''transverse'' region. PYTHIA 6.115 fits the ''transverse'' $\langle N_{\mathrm{chg}}\rangle$ the best, but overshoots slightly the ''toward'' $\langle N_{\mathrm{chg}}\rangle$ in Fig. 23. ISAJET has a lot of activity in the ''transverse'' region, but gives the wrong P_{T1} dependence. Instead of a plateau, ISAJET predicts a rising ''transverse'' $\langle N_{\mathrm{chg}}\rangle$ and gives too much activity at large P_{T1} values. HERWIG does not have enough ''transverse'' $\langle P_T \text{ sum}\rangle$.

We expect the ''transverse'' region to be composed predominately from particles that arise from the breakup of the beam particles and from initial-state radiation. For ISAJET this is clearly the case as can be seen in Fig. 32 where the predictions of ISAJET for the ''transverse'' region are divided into three categories: ''beam-beam remnants,'' initial-state radiation, and outgoing jets plus final-state radiation. It is interesting to see that it is the ''beam-beam remnants'' of ISAJET that are producing the approximately constant plateau. The contributions from initial-state radiation and from the outgoing hard scattering jets both increase as P_{T1} increases. In fact, for ISAJET it is the sharp rise in the initial-state radiation component that is causing the disagreement with the data for $P_{T1}>20$ GeV/c.

As we explained in Sec. II B, for PYTHIA it makes no sense to distinguish particles that arise from initial-state radiation from those that arise from final-state radiation, but one can separate the ''hard scattering component'' from the ''beam-beam remnants.'' Also, for PYTHIA the ''beam-beam remnants'' include contributions from multiple parton scattering as illustrated in Fig. 2. Figure 33 and Fig. 34 compare the ''transverse'' $\langle N_{\mathrm{chg}}\rangle$ with the QCD Monte Carlo model predictions of HERWIG and PYTHIA 6.115, respectively. Here the predictions are divided into two categories: charged particles that arise from the breakup of the beam particles (''beam-beam remnants''), and charged particles that result from the outgoing jets plus initial and final-state radiation (''hard scattering component''). As was the case with ISAJET the ''beam-beam remnants'' form the approximately constant plateau and the ''hard scattering'' component increase as P_{T1}

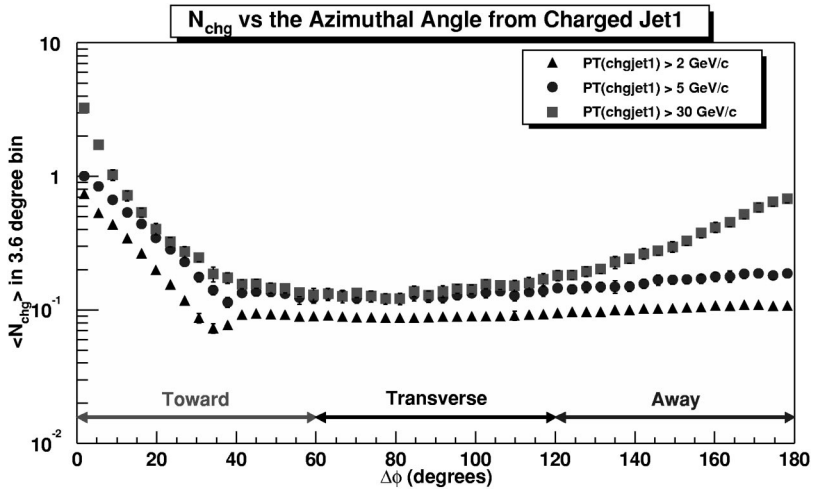

FIG. 15. Average number of charged particles ($p_T>0.5$ GeV/c, $|\eta|<1$) as a function of the relative azimuthal angle, $\Delta\phi$, between the particle and chgjet1 (leading charged jet) for $P_{T1}>2$ GeV/c, 5 GeV/c, and 30 GeV/c. Each point corresponds to the $\langle N_{\mathrm{chg}}\rangle$ in a 3.6° bin. The $P_{T1}>2$ GeV/c and 5 GeV/c points are the min-bias data and the $P_{T1}>30$ GeV/c points are JET20 data. The ''toward,'' ''transverse,'' and ''away'' regions defined in Fig. 14 are labeled.

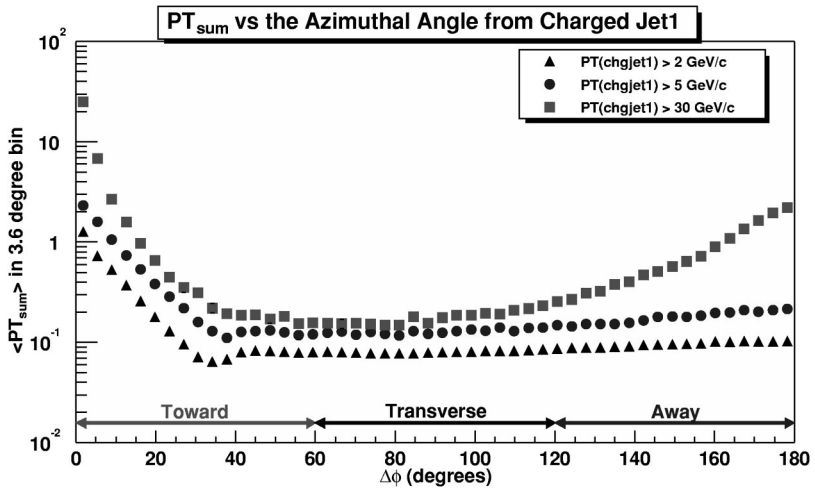

FIG. 16. Average *scalar* p_T sum of charged particles ($p_T>0.5$ GeV/c, $|\eta|<1$) as a function of the relative azimuthal angle, $\Delta\phi$, between the particle and chgjet1 (leading charged jet) for $P_{T1}>2$ GeV/c, 5 GeV/c, and 30 GeV/c. Each point corresponds to the $\langle P_T$ sum$\rangle$ in a 3.6° bin. The $P_{T1}>2$ GeV/c and 5 GeV/c points are the min-bias data and the $P_{T1}>30$ GeV/c points are JET20 data. The ''toward,'' ''transverse,'' and ''away'' regions defined in Fig. 14 are labeled.

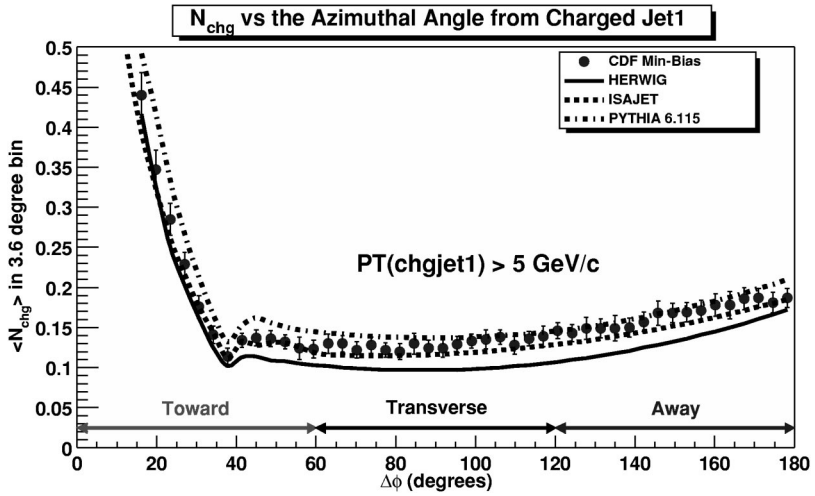

FIG. 17. Data from Fig. 15 on the average number of charged particles ($p_T>0.5$ GeV/c, $|\eta|<1$) as a function of the relative azimuthal angle, $\Delta\phi$, between the particle and chgjet1 (leading charged jet) for $P_{T1}>5$ GeV/c compared to QCD Monte Carlo model predictions of HERWIG, ISAJET, and PYTHIA 6.115. The ''toward,'' ''transverse,'' and ''away'' regions defined in Fig. 14 are labeled.

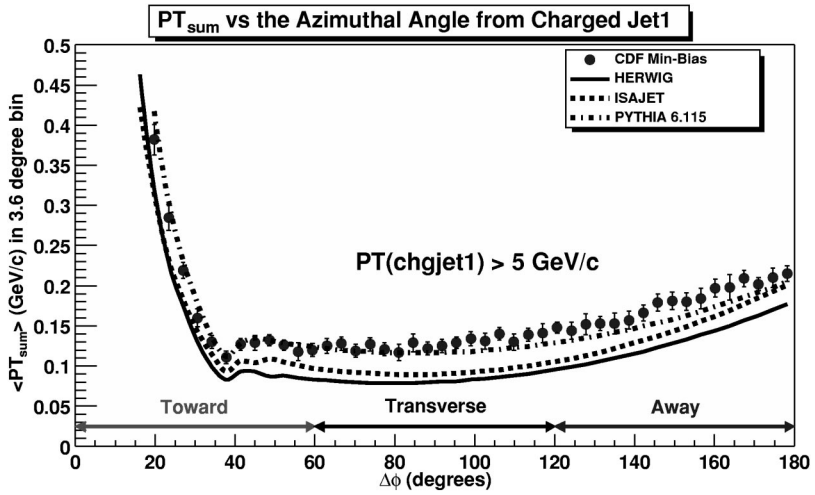

FIG. 18. Data from Fig. 16 on the average *scalar* p_T sum of charged particles ($p_T>0.5$ GeV/c, $|\eta|<1$) as a function of the relative azimuthal angle, $\Delta\phi$, between the particle and chgjet1 (leading charged jet) for $P_{T1}>5$ GeV/c compared to QCD Monte Carlo model predictions of HERWIG, ISAJET, and PYTHIA 6.115. The ''toward,'' ''transverse,'' and ''away'' regions defined in Fig. 14 are labeled.

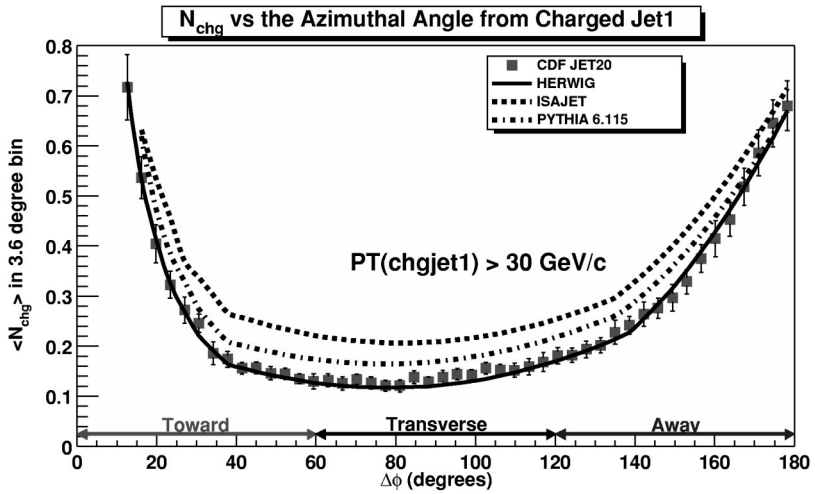

FIG. 19. Data from Fig. 15 on the average number of charged particles ($p_T>0.5$ GeV/c, $|\eta|<1$) as a function of the relative azimuthal angle, $\Delta\phi$, between the particle and chgjet1 (leading charged jet) for $P_{T1}>30$ GeV/c compared to QCD Monte Carlo model predictions of HERWIG, ISAJET, and PYTHIA 6.115. The ''toward,'' ''transverse,'' and ''away'' regions defined in Fig. 14 are labeled.

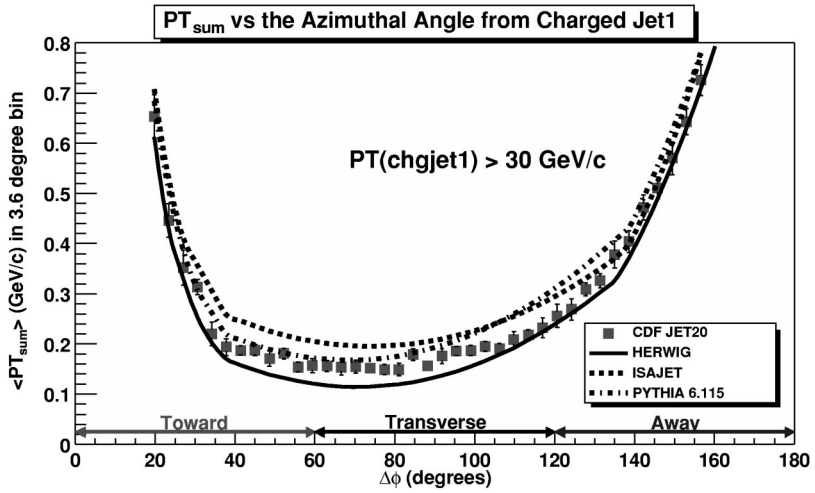

FIG. 20. Data from Fig. 16 on the average *scalar* p_T sum of charged particles ($p_T>0.5$ GeV/c, $|\eta|<1$) as a function of the relative azimuthal angle, $\Delta\phi$, between the particle and chgjet1 (leading charged jet) for $P_{T1}>30$ GeV/c compared to QCD Monte Carlo model predictions of HERWIG, ISAJET, and PYTHIA 6.115. The ''toward,'' ''transverse,'' and ''away'' regions defined in Fig. 14 are labeled.

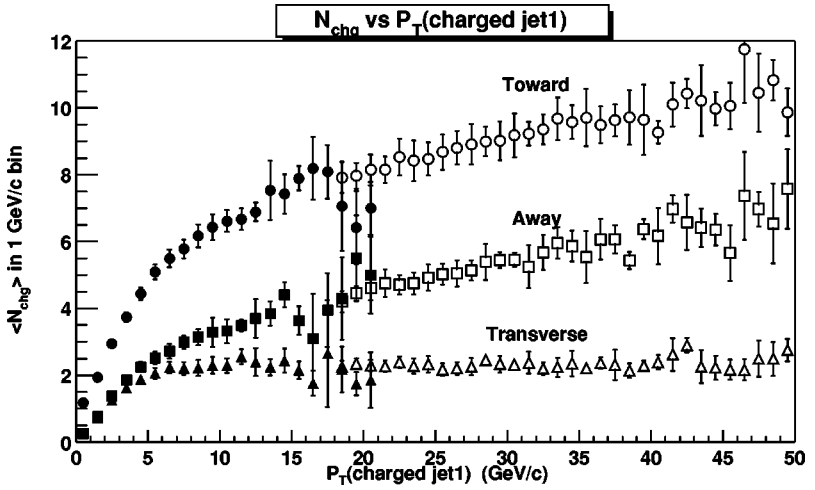

FIG. 21. The average number of ''toward'' ($|\Delta\phi|<60°$), ''transverse'' ($60°<|\Delta\phi|<120°$), and ''away'' ($|\Delta\phi|>120°$) charged particles ($p_T>0.5$ GeV/c, $|\eta|<1$, including chgjet1) as a function of the transverse momentum of the leading charged jet. Each point corresponds to the $\langle N_{\rm chg}\rangle$ in a 1 GeV/c bin. The solid (open) points are the min-bias (JET20) data. The errors on the (uncorrected) data include both statistical and correlated systematic uncertainties. The ''toward,'' ''transverse,'' and ''away'' regions are illustrated in Fig. 14 and labeled in Fig. 15.

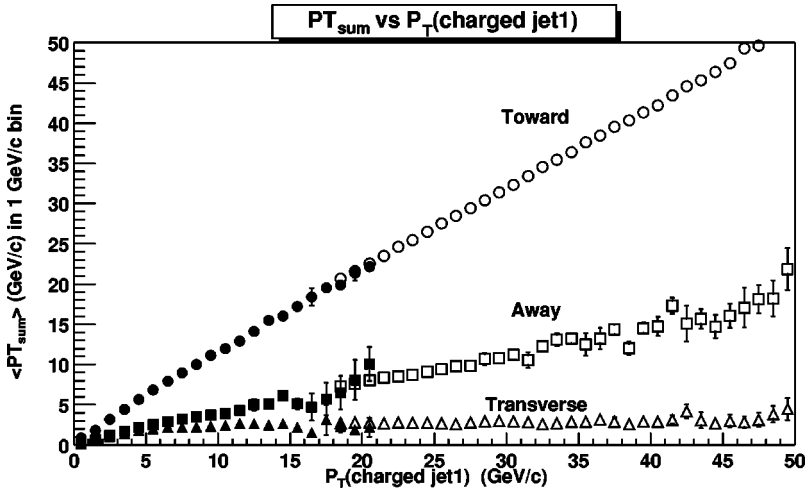

FIG. 22. The average *scalar* p_T sum of "toward" ($|\Delta\phi|<60°$), "transverse" ($60°<|\Delta\phi|<120°$), and "away" ($|\Delta\phi|>120°$) charged particles ($p_T>0.5$ GeV/c, $|\eta|<1$, including chgjet1) as a function of the transverse momentum of the leading charged jet. Each point corresponds to the $\langle P_T \text{ sum}\rangle$ in a 1 GeV/c bin. The solid (open) points are the min-bias (JET20) data. The errors on the (uncorrected) data include both statistical and correlated systematic uncertainties. The "toward," "transverse," and "away" regions are illustrated in Fig. 14 and labeled in Fig. 16.

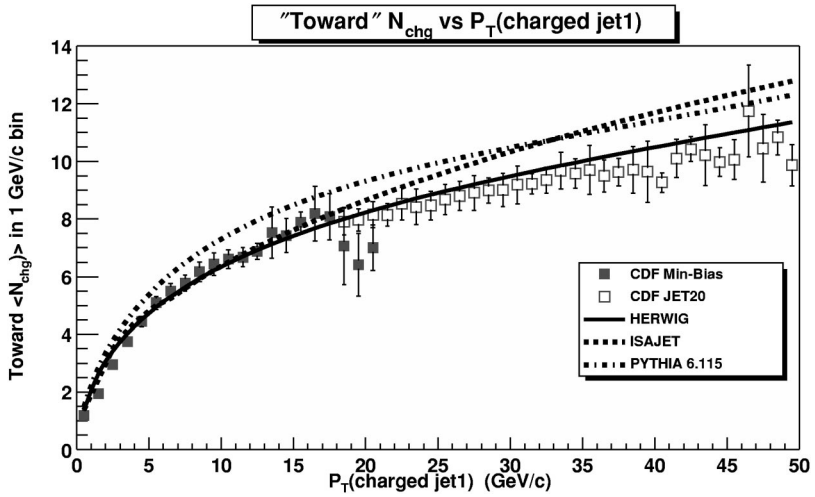

FIG. 23. Data from Fig. 21 on the average number of charged particles ($p_T>0.5$ GeV/c, $|\eta|<1$) as a function of P_{T1} (leading charged jet) for the "toward" region defined in Fig. 14 compared with the QCD Monte Carlo model predictions of HERWIG, ISAJET, and PYTHIA 6.115.

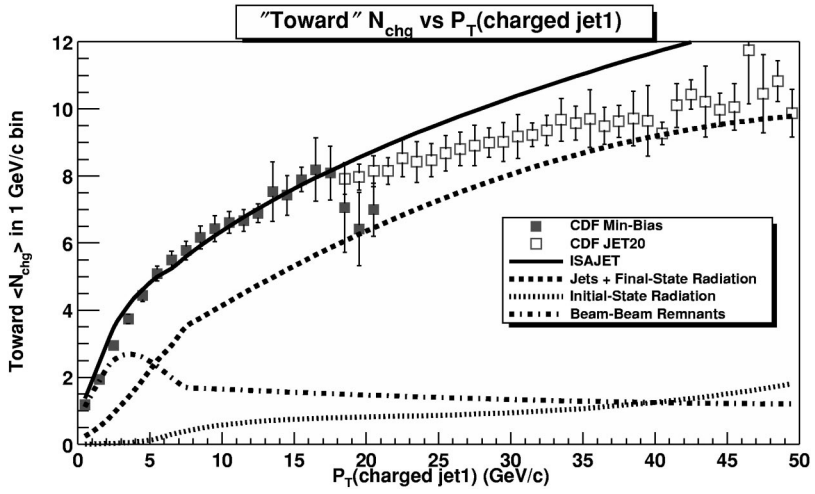

FIG. 24. Data from Fig. 21 on the average number of charged particles ($p_T>0.5$ GeV/c, $|\eta|<1$) as a function of P_{T1} (leading charged jet) for the "toward" region defined in Fig. 14 compared with the QCD Monte Carlo model predictions of ISAJET. The predictions of ISAJET are divided into three categories: charged particles that arise from the breakup of the beam particles ("beam-beam remnants"), charged particles that arise from initial-state radiation, and charged particles that result from the outgoing jets plus final-state radiation (see Fig. 1).

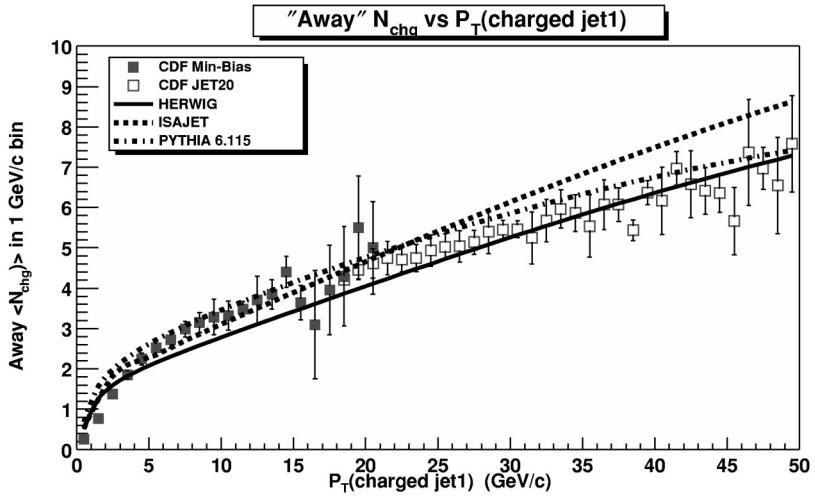

FIG. 25. Data from Fig. 21 on the average number of charged particles ($p_T>0.5$ GeV/c, $|\eta|<1$) as a function of P_{T1} (leading charged jet) for the ''away'' region defined in Fig. 14 compared with the QCD Monte Carlo model predictions of HERWIG, ISAJET, and PYTHIA 6.115. The solid (open) points are the min-bias (JET20) data.

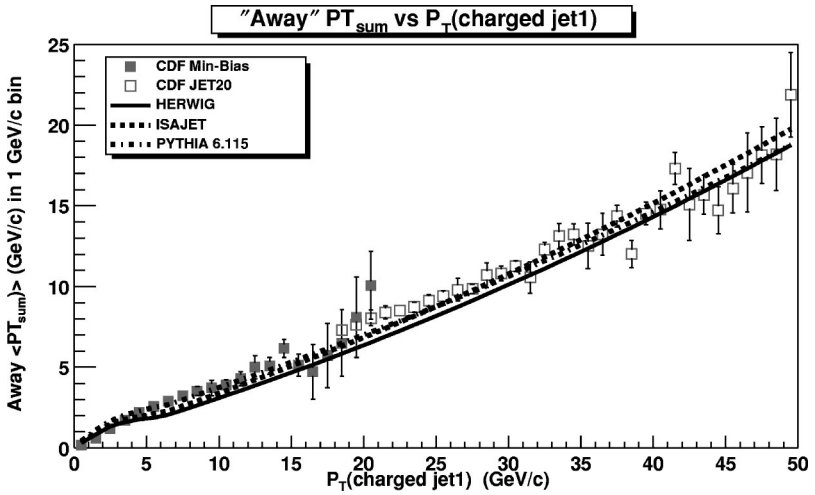

FIG. 26. Data from Fig. 22 on the average *scalar* p_T sum of charged particles ($p_T>0.5$ GeV/c, $|\eta|<1$) as a function of P_{T1} (leading charged jet) for the ''away'' region defined in Fig. 14 compared with the QCD Monte Carlo model predictions of HERWIG, ISAJET, and PYTHIA 6.115.

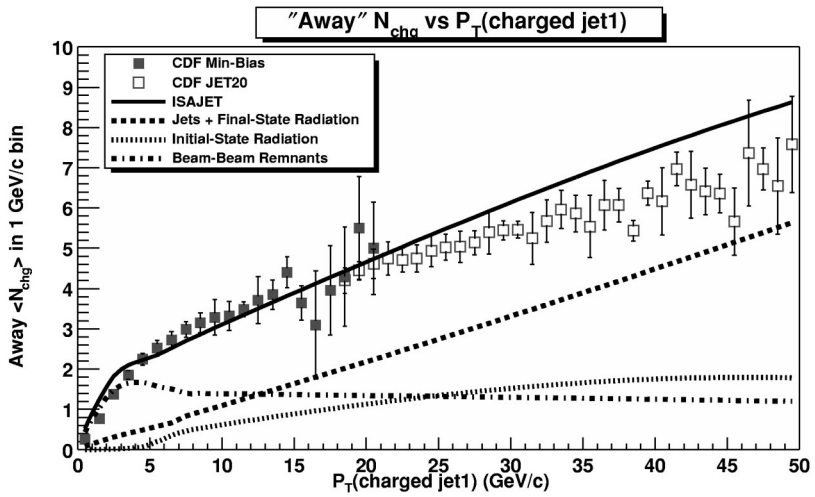

FIG. 27. Data from Fig. 21 on the average number of charged particles ($p_T>0.5$ GeV/c, $|\eta|<1$) as a function of P_{T1} (leading charged jet) for the ''away'' region defined in Fig. 14 compared with the QCD Monte Carlo model predictions of ISAJET. The predictions of ISAJET are divided into three categories: charged particles that arise from the breakup of the beam particles (''beam-beam remnants''), charged particles that arise from initial-state radiation, and charged particles that result from the outgoing jets plus final-state radiation (see Fig. 1).

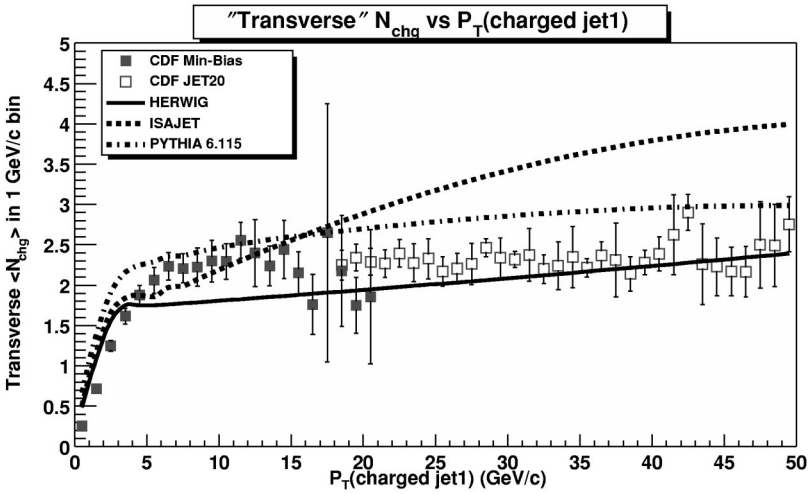

FIG. 28. Data from Fig. 21 on the average number of charged particles ($p_T>0.5$ GeV/c, $|\eta|<1$) as a function of P_{T1} (leading charged jet) for the ''transverse'' region defined in Fig. 14 compared with the QCD Monte Carlo model predictions of HERWIG, ISAJET, and PYTHIA 6.115. The solid (open) points are the min-bias (JET20) data.

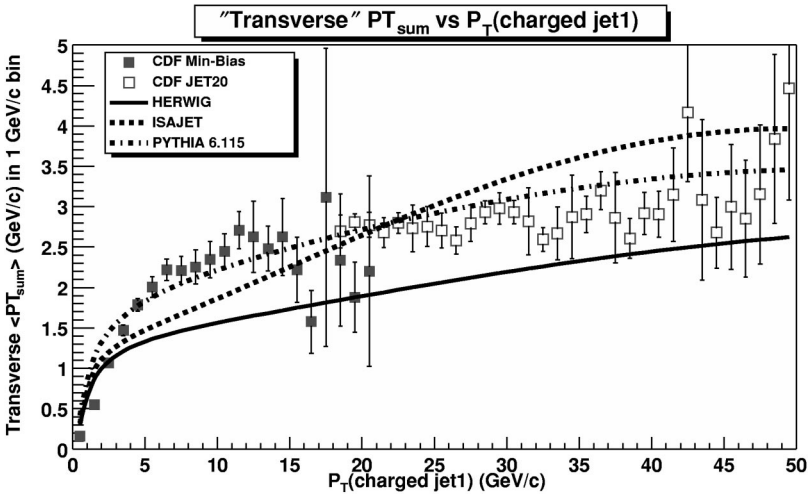

FIG. 29. Data from Fig. 22 on the average *scalar* p_T sum of charged particles ($p_T>0.5$ GeV/c, $|\eta|<1$) as a function of P_{T1} (leading charged jet) for the ''transverse'' region defined in Fig. 14 compared with the QCD Monte Carlo model predictions of HERWIG, ISAJET, and PYTHIA 6.115.

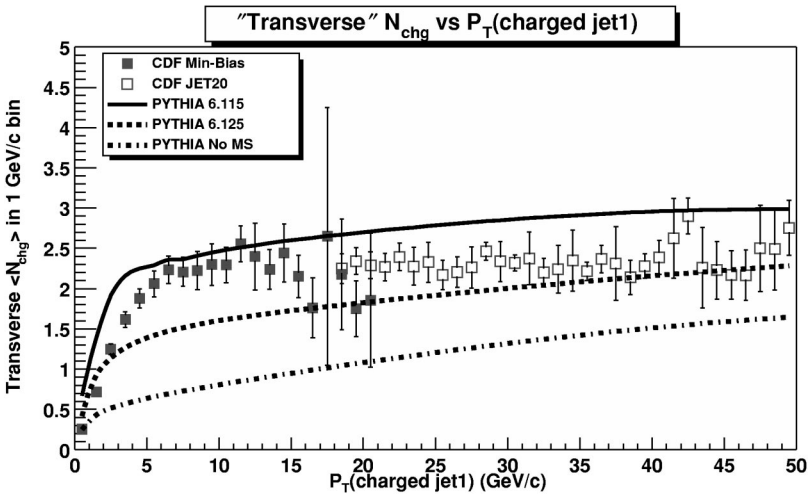

FIG. 30. Data from Fig. 21 on the average number of charged particles ($p_T>0.5$ GeV/c, $|\eta|<1$) as a function of P_{T1} (leading charged jet) for the ''transverse'' region defined in Fig. 14 compared with the QCD Monte Carlo model predictions of PYTHIA 6.115, PYTHIA 6.125, and PYTHIA 6.115 with no multiple parton scattering (no MS).

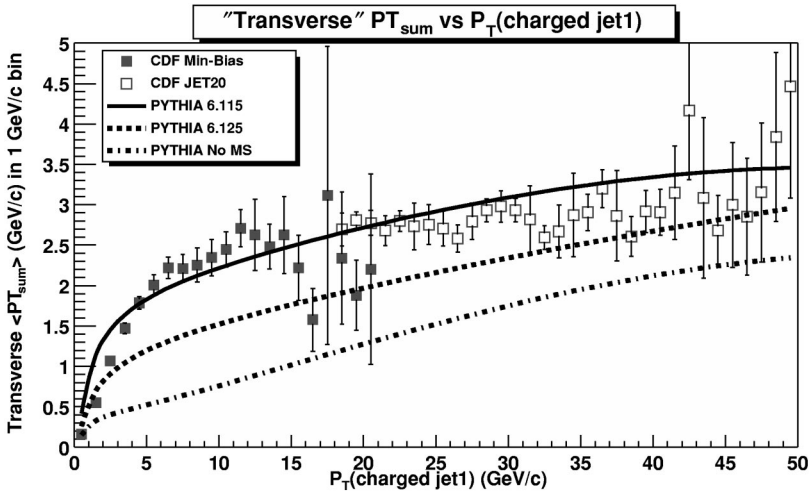

FIG. 31. Data from Fig. 22 on the average *scalar* p_T sum of charged particles ($p_T > 0.5$ GeV/c, $|\eta| < 1$) as a function of P_{T1} (leading charged jet) for the ''transverse'' region defined in Fig. 14 compared with the QCD Monte Carlo model predictions of PYTHIA 6.115, PYTHIA 6.125, and PYTHIA with no multiple parton scattering (no MS).

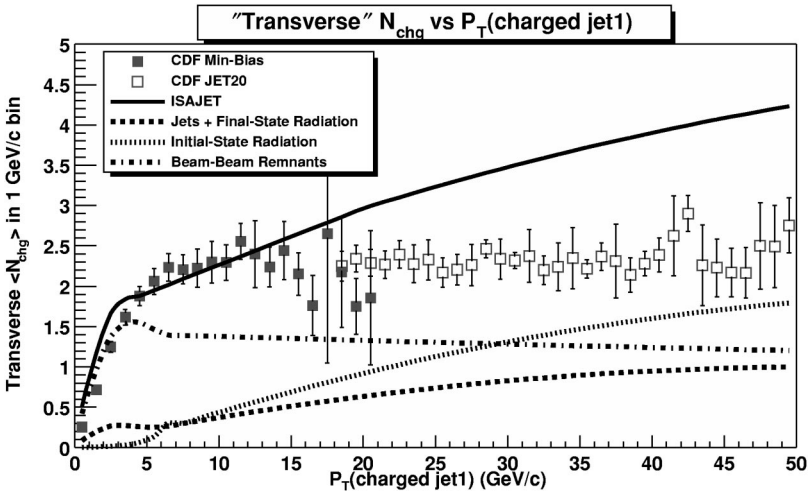

FIG. 32. Data from Fig. 21 on the average number of charged particles ($p_T > 0.5$ GeV/c, $|\eta| < 1$) as a function of P_{T1} (leading charged jet) for the ''transverse'' region defined in Fig. 14 compared with the QCD Monte Carlo model predictions of ISAJET. The predictions of ISAJET are divided into three categories: charged particles that arise from the breakup of the beam particles (''beam-beam remnants''), charged particles that arise from initial-state radiation, and charged particles that result from the outgoing jets plus final-state radiation (see Fig. 1).

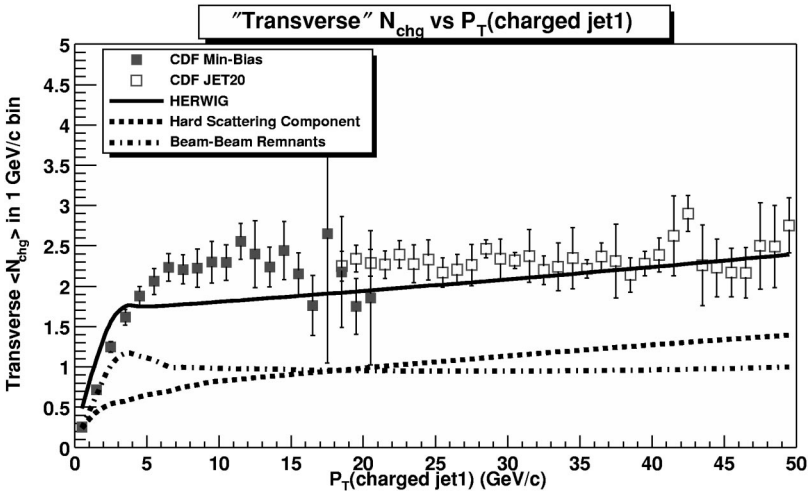

FIG. 33. Data from Fig. 21 on the average number of charged particles ($p_T > 0.5$ GeV/c, $|\eta| < 1$) as a function of P_{T1} (leading charged jet) for the ''transverse'' region defined in Fig. 14 compared with the QCD Monte Carlo model predictions of HERWIG. The predictions of HERWIG are divided into two categories: charged particles that arise from the breakup of the beam particles (''beam-beam remnants''), and charged particles that result from the outgoing jets plus initial and final-state radiation (''hard scattering component'') (see Fig. 1).

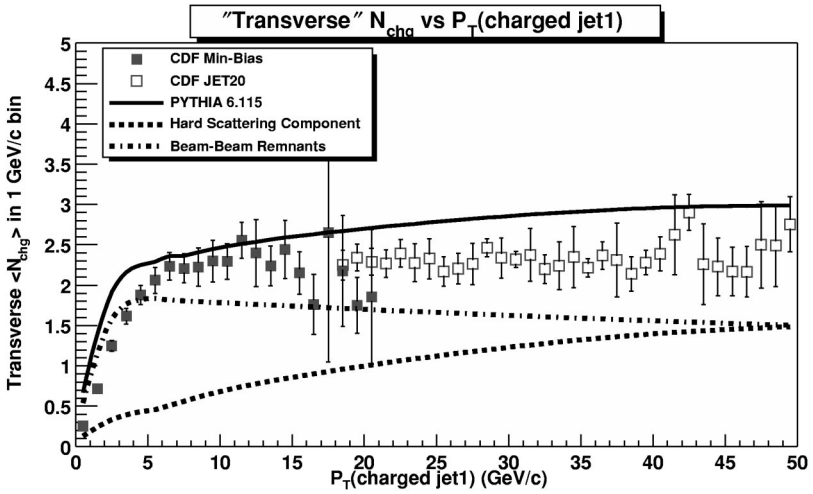

FIG. 34. Data from Fig. 21 on the average number of charged particles ($p_T>0.5$ GeV/c, $|\eta|<1$) as a function of P_{T1} (leading charged jet) for the ''transverse'' region defined in Fig. 14 compared with the QCD Monte Carlo model predictions of PYTHIA 6.115. The predictions of PYTHIA are divided into two categories: charged particles that arise from the breakup of the beam particles (''beam-beam remnants''), and charged particles that result from the outgoing jets plus initial and final-state radiation (''hard scattering component''). For PYTHIA the ''beam-beam remnants'' include contributions from multiple parton scattering (see Fig. 2).

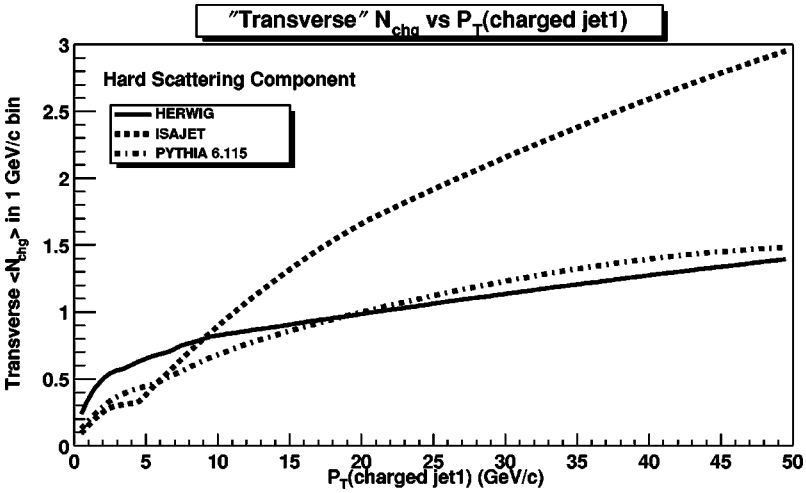

FIG. 35. QCD Monte Carlo model predictions from HERWIG, ISAJET, and PYTHIA 6.115 of the average number of charged particles ($p_T>0.5$ GeV/c, $|\eta|<1$) as a function of P_{T1} (leading charged jet) for the ''transverse'' region defined in Fig. 14 arising from the outgoing jets plus initial and final-state radiation (''hard scattering component'').

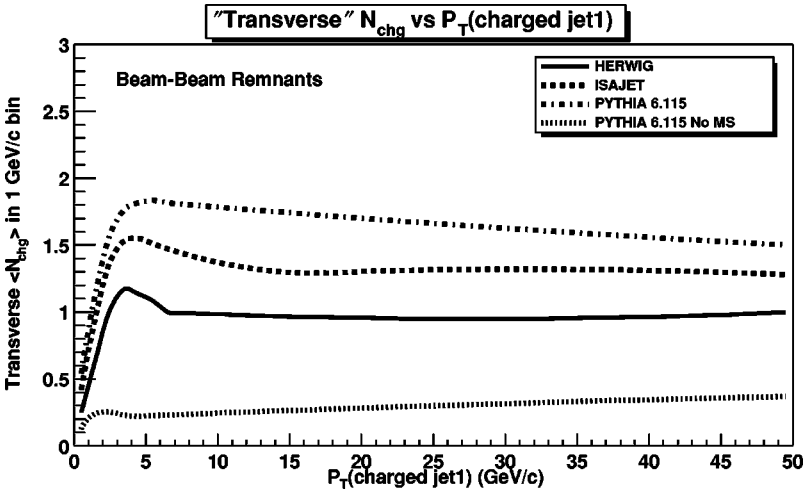

FIG. 36. QCD Monte Carlo model predictions from HERWIG, ISAJET, PYTHIA 6.115, and PYTHIA 6.115 with no multiple parton scattering (no MS) for the average number of charged particles ($p_T>0.5$ GeV/c, $|\eta|<1$) as a function of P_{T1} (leading charged jet) for the ''transverse'' region defined in Fig. 14 arising from the breakup of the beam particles (''beam-beam remnants''). For PYTHIA the ''beam-beam remnants'' include contributions from multiple parton scattering (see Fig. 2).

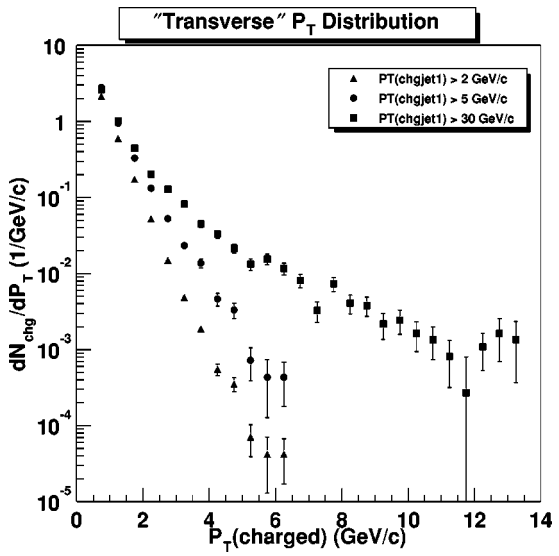

FIG. 37. Data on the transverse momentum distribution of charged particles ($p_T>0.5$ GeV/c, $|\eta|<1$) in the ''transverse'' region defined in Fig. 14 for $P_{T1}>2$ GeV/c, 5 GeV/c, and 30 GeV/c, where chgjet1 is the leading charged particle jet. The $P_{T1}>2$ GeV/c and 5 GeV/c points are min-bias data and the $P_{T1}>30$ GeV/c are JET20 data. Each point corresponds to the charged particle density $d\langle N_{\rm chg}\rangle/dp_T$ and the integral of the distribution gives the average number of charged particles in the ''transverse'' region, $\langle N_{\rm chg}({\rm transverse})\rangle$. The errors on the (uncorrected) data include both statistical and correlated systematic uncertainties.

increases. However, the ''hard scattering'' component of HERWIG and PYTHIA does not rise nearly as fast as the ''hard scattering'' component of ISAJET. This can be seen clearly in Fig. 35 where we compare directly the ''hard scattering'' component (outgoing jets plus initial and final-state radiation) of the ''transverse'' $\langle N_{\rm chg}\rangle$ from ISAJET, HERWIG, and PYTHIA 6.115. PYTHIA and HERWIG are similar and rise gently as P_{T1} increases, whereas ISAJET produces a much sharper increase as P_{T1} increases. There are two reasons why the ''hard scattering'' component of ISAJET is different from HERWIG and PYTHIA. The first is due to different fragmentation schemes. ISAJET uses independent fragmentation, which produces too many soft hadrons when partons begin to overlap. The second difference arises from the way the QCD Monte Carlo models produce parton showers. ISAJET uses a leading-log picture in which the partons within the shower are ordered according to their invariant mass. Kinematics requires that the invariant mass of daughter partons be less than the invariant mass of the parent. HERWIG and PYTHIA modify the leading-log picture to include color coherence effects which leads to angle ordering within the parton shower. Angle ordering produces less high p_T radiation within a parton shower which is what is seen in Fig. 35. Without further study, we do not know how much of the difference seen in Fig. 35 is due to the different fragmentation schemes and how much is due to color coherence effects.

The ''beam-beam remnant'' contribution to the ''transverse'' $\langle N_{\rm chg}\rangle$ is different for each of the QCD Monte Carlo models. This can be seen in Fig. 36 where we compare directly the ''beam-beam remnant'' component of the ''transverse'' $\langle N_{\rm chg}\rangle$ from ISAJET, HERWIG, PYTHIA 6.115, and PYTHIA with no multiple parton interactions. Since we are considering only charged particles with $p_T>0.5$ GeV/c, the height of the plateaus in Fig. 36 is related to the transverse momentum distribution of the ''beam-beam remnant'' contributions. A steeper p_T distribution means less particles with $p_T>0.5$ GeV/c. PYTHIA uses multiple parton scattering to enhance the ''underlying event'' and we have included these contributions in the ''beam-beam remnants.'' For PYTHIA the height of the plateau in Fig. 36 can be adjusted by adjusting the amount of multiple parton scattering. HERWIG and ISAJET do not include multiple parton scattering. For HERWIG and ISAJET the height of the plateau can be adjusted by changing the p_T distribution of the ''beam-beam remnants.''

B. "Transverse" p_T distribution

Figure 37 shows the data on the transverse momentum distribution of charged particles ($|\eta|<1$) in the ''transverse'' region, where p_T is measured with respect to the beam axis. The $P_{T1}>2$ GeV/c and 5 GeV/c points are min-bias data and the $P_{T1}>30$ GeV/c points are JET20 data. Each point corresponds to the charged particle density $d\langle N_{\rm chg}\rangle/dp_T$ and the integral of the distribution gives the average number of charged particles in the ''transverse'' region, $\langle N_{\rm chg}({\rm transverse})\rangle$. Since these distributions fall off sharply as p_T increases, it is essentially only the first few points at low p_T that determines $\langle N_{\rm chg}({\rm transverse})\rangle$. The approximately constant plateau seen in Fig. 28 is a result of the low p_T points in Fig. 37 not changing much as P_{T1} changes. However, the high p_T points in Fig. 37 do increase considerably as P_{T1} increases. This effect cannot be seen by simply examining the average number of ''transverse'' particles. Figure 37 shows the growth of the ''hard scattering'' component in the ''transverse'' region (i.e., three or more hard scattering jets).

For the Monte Carlo models, at low values of P_{T1} the p_T distribution in the ''transverse'' region is dominated by the ''beam-beam remnant'' contribution with very little hard scattering. This can be seen in Fig. 38 which shows both the ''beam-beam remnant'' component and the total prediction of HERWIG for $P_{T1}>2$ GeV/c. For the Monte Carlo models, the p_T distribution in the ''transverse'' region at low values of P_{T1} measures directly the p_T distribution of the ''beam-beam remnants'' component. Figure 39 compares the predictions of HERWIG, ISAJET, and PYTHIA with the data from Fig. 37 for $P_{T1}>2$ GeV/c. Both ISAJET and HERWIG have the wrong p_T dependence due to ''beam-beam remnant'' components that fall off too rapidly as p_T increases. PYTHIA does a better job, but is still too steep. It is, of course, understandable that the Monte Carlo models might be slightly off on the parameterization of the ''beam-beam remnants.'' This component cannot be calculated from perturbation theory and must be determined from data.

Figure 40 shows both the ''beam-beam remnant'' component and the total prediction of HERWIG for $P_{T1}>30$ GeV/c. Here there is a large ''hard scattering'' component corresponding to the production of more than two large p_T jets. In Fig. 41 we compare the predictions of HERWIG, ISAJET, and

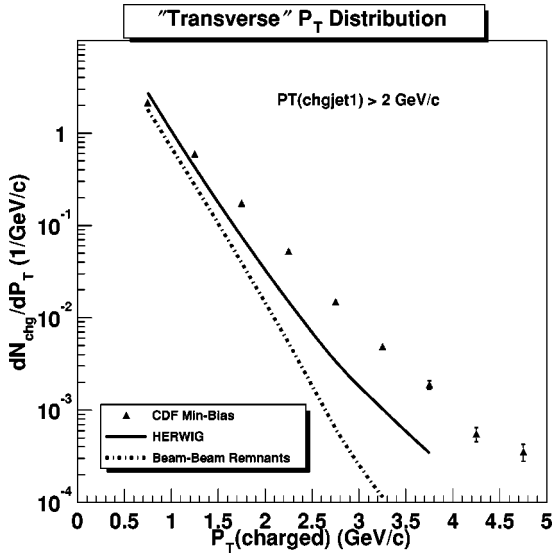

FIG. 38. Data from Fig. 37 on the transverse momentum distribution of charged particles ($p_T>0.5$ GeV/c, $|\eta|<1$) in the ''transverse'' region defined in Fig. 14 for $P_{T1}>2$ GeV/c compared to the QCD hard scattering Monte Carlo model predictions from HERWIG. The dashed curve shows the contribution arising from the breakup of the beam particles (''beam-beam remnants'') predicted by HERWIG.

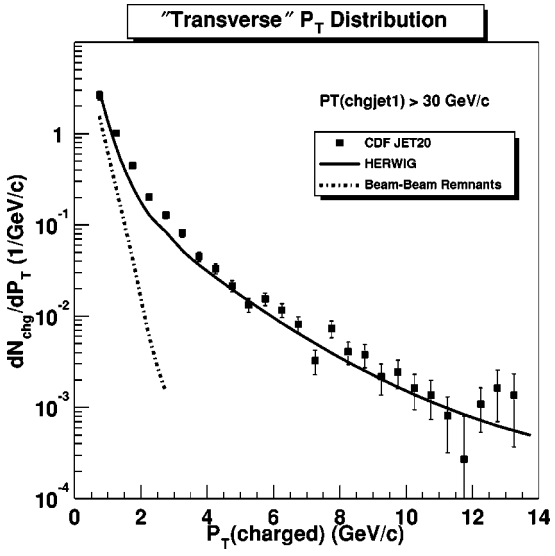

FIG. 40. Data from Fig. 37 on the transverse momentum distribution of charged particles ($p_T>0.5$ GeV/c, $|\eta|<1$) in the ''transverse'' region defined in Fig. 14 for $P_{T1}>30$ GeV/c compared to the QCD hard scattering Monte Carlo model predictions from HERWIG. The dashed curve shows the contribution arising from the breakup of the beam particles (''beam-beam remnants'') predicted by HERWIG.

PYTHIA 6.115 with the data from Fig. 37 for $P_{T1}>30$ GeV/c. All the models do well at describing the high p_T tail of this distribution. However, ISAJET produces too many charged particles at low p_T. This is a result of the wrong p_T dependence for the ''beam-beam remnant'' contribution and from an overabundance of soft particles produced in the ''hard scattering.'' This shows that the large rise in the ''transverse'' charged multiplicity from the ''hard scattering'' component of ISAJET seen in Fig. 35 comes from soft particles. This is to be expected from a model that employs independent fragmentation such as ISAJET. Independent fragmentation does not differ much from color string or cluster fragmentation for the hard particles, but independent fragmentation produces too many soft particles.

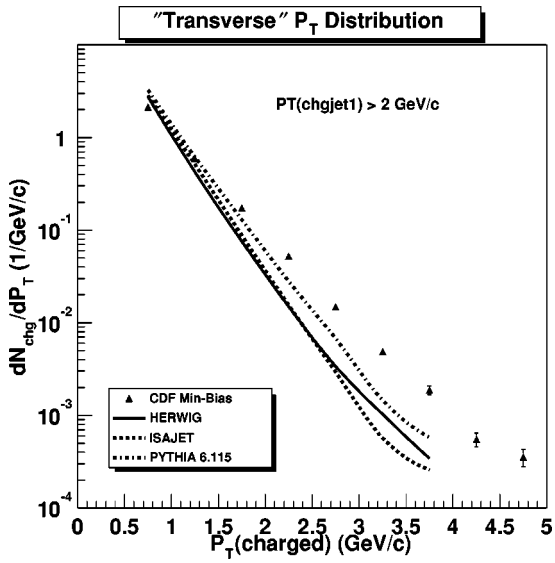

FIG. 39. Data from Fig. 37 on the transverse momentum distribution of charged particles ($p_T>0.5$ GeV/c, $|\eta|<1$) in the ''transverse'' region defined in Fig. 14 for $P_{T1}>2$ GeV/c compared to the QCD hard scattering Monte Carlo model predictions from predictions from HERWIG, ISAJET, and PYTHIA 6.115.

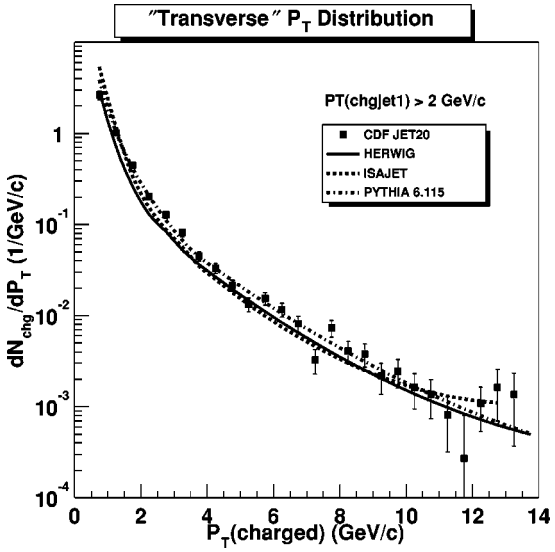

FIG. 41. Data from Fig. 37 on the transverse momentum distribution of charged particles ($p_T>0.5$ GeV/c, $|\eta|<1$) in the ''transverse'' region defined in Fig. 14 for $P_{T1}>30$ GeV/c compared to the QCD hard scattering Monte Carlo model predictions from predictions from HERWIG, ISAJET, and PYTHIA 6.115.

VI. SUMMARY AND CONCLUSIONS

We have studied observables that describe the leading charged jet and observables that are sensitive to the overall event structure in proton-antiproton collisions at 1.8 TeV. Our summary and conclusions are as follows.

The evolution of charged particle jets. We see evidence of charged particle clusters (i.e., charged particle jets) in the min-bias data. These charged particle jets become apparent around P_{T1} of 2 GeV/c with, on the average, about 2 charged particles with $p_T > 0.5$ GeV/c and $|\eta| < 1$ and grow to, on the average, about 10 charged particles with $p_T > 0.5$ GeV/c and $|\eta| < 1$ at $P_{T1} = 50$ GeV/c. The QCD Monte Carlo models describe quite well (although not perfectly) leading charged jet observables such as the multiplicity distribution of charged particles within the leading charged jet, the size of the leading charged jet, the radial distribution of charged particles and transverse momentum around the leading charged jet direction, and the momentum distribution of charged particles within the leading charged jet. In fact, the QCD Monte Carlo models agree as well with 5 GeV/c charged particle jets as they do with 50 GeV/c charged particle jets. The charged particle jets in the min-bias data are simply a continuation (down to small p_T) of the high transverse momentum charged jets observed in the JET20 data.

The "underlying event." For the QCD Monte Carlo models, a hard scattering collider event consists of large transverse momentum outgoing hadrons that originate from the large transverse momentum partons (*outgoing jets*) and also hadrons that originate from the breakup of the proton and antiproton ("beam-beam remnants"). The "underlying event" is everything except the two outgoing hard scattered jets and receives contributions from the "beam-beam remnants" plus initial and final-state radiation, and possibly from "soft" or "semi-hard" multiple parton interactions. If we assume that the "transverse" region is a good measurement of the "underlying event" as the QCD Monte Carlo models suggest, then our data show that the average number of charged particles and average charged *scalar* p_T sum in the "underlying event" grows very rapidly with the transverse momentum of the leading charged particle jet and then forms an approximately constant plateau for $P_{T1} > 5$ GeV/c. The height of this plateau is at least twice that observed in ordinary "soft" collisions at the same energy.

None of the QCD Monte Carlo models we examined correctly describe all the properties of the "transverse" region seen in the data. HERWIG and PYTHIA 6.125 do not have enough activity in the "transverse" region. PYTHIA 6.115 has about the right amount of activity in the "transverse" region, but produces too much overall charged multiplicity. ISAJET has a lot of activity in the "transverse" region, but with the wrong dependence on P_{T1}. Because ISAJET uses independent fragmentation and HERWIG and PYTHIA do not, there are clear differences in the "hard scattering" component (mostly initial-state radiation) of the "underlying event" between ISAJET and the other two Monte Carlo models. Here the data strongly favor HERWIG and PYTHIA over ISAJET.

In QCD Monte Carlo models, the p_T distribution in the "transverse" region for low values of P_{T1} measures directly the p_T distribution of the "beam-beam remnants." Our data indicate that the "beam-beam remnant" component of both ISAJET and HERWIG has the wrong p_T dependence. ISAJET and HERWIG both predict a p_T distribution for the "beam-beam remnants" that is too steep. With multiple parton interactions included, PYTHIA does a better job but still has a p_T distribution for the "beam-beam remnants" that is slightly too steep. It is, of course, understandable that the Monte Carlo models might be somewhat off on the parametrization of the "beam-beam remnants." This component cannot be calculated from perturbation theory and must be determined from data. With what we have learned from the data presented here, the "beam-beam remnant" component and the multiple parton scattering component of the QCD Monte Carlo models can be tuned to better describe the "underlying event" in proton-antiproton collisions.

ACKNOWLEDGMENTS

We thank the Fermilab staff and the technical staffs of the participating institutions for their vital contributions. This work is supported by the U.S. Department of Energy and the National Science Foundation; the Natural Sciences and Engineering Research Council of Canada; the Istituto Nazionale di Fisica Nucleare of Italy; the Ministry of Education, Science and Culture of Japan; the National Science Council of the Republic of China; and the A.P. Sloan Foundation.

[1] G. Marchesini and B.R. Webber, Nucl. Phys. **B310**, 461 (1988); I.G. Knowles, *ibid.* **B310**, 571 (1988); S. Catani, G. Marchesini, and B.R. Webber, *ibid.* **B349**, 635 (1991).

[2] F. Paige and S. Protopopescu, BNL Report BNL38034, 1986, version 7.32.

[3] T. Sjostrand, Phys. Lett. **157B**, 321 (1985); M. Bengtsson, T. Sjostrand, and M. van Zijl, Z. Phys. C **32**, 67 (1986); T. Sjostrand and M. van Zijl, Phys. Rev. D **36**, 2019 (1987).

[4] In CDF the positive z axis lies along the incident proton beam direction, ϕ is the azimuthal angle, θ is the polar angle, and $p_T = \sqrt{p_x^2 + p_y^2}$. The pseudorapidity, η, is defined as $-\ln[\tan(\theta/2)]$.

[5] F. Abe *et al.*, Nucl. Instrum. Methods Phys. Res. A **271**, 387 (1988); F. Bedeshi *et al.*, *ibid.* **268**, 50 (1988).

[6] F. Abe *et al.*, Phys. Rev. D **56**, 3811 (1997); F. Abe *et al.*, Phys. Rev. Lett. **79**, 584 (1997).

[7] R.D. Field and R.P. Feynman, Nucl. Phys. **B136**, 1 (1978).

[8] F. Abe *et al.*, Phys. Rev. D **41**, 2330 (1990).